

Volume 4 Issue 2
December 2022

MERSIN PHOTOGRAMMETRY JOURNAL



EDITOR IN CHIEF

Prof. Dr. Murat YAKAR
Mersin University, Engineering Faculty
Turkey

CO-EDITORS

Assist. Prof. Dr. Ali ULVI
Mersin University, Engineering Faculty
Turkey

ADVISORY BOARD

Prof. Dr. Orhan ALTAN
Honorary Member of ISPRS, ICSU EB Member
Turkey

Prof. Dr. Naser El SHAMY
The University of Calgary Department of Geomatics Engineering,
Canada

Prof. Dr. Armin GRUEN
ETH Zurich University
Switzerland

Prof. Dr. Ferruh YILDIZ
Konya Technical University
Faculty of Engineering and Natural Sciences
Turkey

EDITORIAL BOARD

Prof. Dr. Alper YILMAZ
Environmental and Geodetic Engineering, The Ohio State University,
USA

Prof. Dr. Dieter FRITSCH
University of Stuttgart Institute for Photogrammetry
Germany

Prof. Dr. Petros PATIAS
The Aristotle University of Thessaloniki, Faculty of Rural & Surveying Engineering
Greece

Prof. Dr. Pierre GRUSSENMEYER
National Institute of Applied Science, Department of civil engineering and surveying
France

Prof. Dr. Xiaoli DING
The Hong Kong Polytechnic University, Faculty of Construction and Environment
Hong Kong

Dr. Hsiu-Wen CHANG
National Cheng Kung University, Department of Geomatics
Taiwan

Prof. Dr. Rey-Jer YOU
National Cheng Kung University, Tainan · Department of Geomatics,
China

Prof. Dr. Bülent BAYRAM
Yıldız Technical University Engineering Faculty,
Turkey

Prof. Dr. İbrahim YILMAZ
Afyon Kocatepe University Engineering Faculty,
Turkey

Prof. Dr. Ömer MUTLUOĞLU
Konya Technical University
Faculty of Engineering and Natural Sciences,
Turkey

Dr. Öğr. Üyesi, Nizar POLAT
Harran University, Engineering Faculty,
Turkey

Dr. Öğr. Üyesi. Sefa BİLGİLİOĞLU
Aksaray University, Engineering Faculty,
Turkey

Dr. Surendra Pal Singh,
Ethiopian Government University
Ethiopia

Dr. Dereje Sufa,
Wollega University
Ethiopia

The MERSİN PHOTOGRAMMETRY JOURNAL (MEPHOJ)

THE MERSİN PHOTOGRAMMETRY JOURNAL (MEPHOJ) publishes original and innovative contributions in photogrammetric applications ranging from the integration of instruments, methodologies, and technologies and their respective uses in the environmental sciences, engineering, and other natural sciences. Mersin Photogrammetry Journal is a branch of science that widely applied in many scientific disciplines. MEPHOJ aims to cover the entirety of Photogrammetry and Photogrammetric applications about Geosciences, including their application domains. MEPHOJ strives to encourage scientists to publish experimental, theoretical, and computational results as detailed as possible so that results can be easily reproduced.

MEPHOJ is a double peer-reviewed (blind) OPEN ACCESS JOURNAL that publishes professional level research articles and subject reviews exclusively in English. It allows authors to submit articles online and track his or her progress via its web interface. All manuscripts will undergo a refereeing process; acceptance for publication is based on at least two positive reviews. The journal publishes research and review papers, professional communication, and technical notes. MEPHOJ does not charge for any article submissions or for processing.

CORRESPONDENCE ADDRESS
Journal Contact: myakar@mersin.edu.tr

CONTENTS

Volume 4 - Issue 2

RESEARCH ARTICLES

** Automated measurement of carotid angle with use of CT images

Nusret Demir, Serkan Demir 37-44

** Use of unmanned aerial vehicle (UAV) for mapping, and accuracy assessment of the orthophoto with and without using GCPs: A case study in Nepal

Abinash Silwal, Sunil Tamang, Rajendra Adhikari 45-52

** Detection and documentation of stone material deterioration in historical masonry buildings using UAV photogrammetry: A case study of Mersin Sarisih Inn

Lale Karataş, Aydın Alptekin, Atilla Karabacak, Murat Yakar 53-61

** Application of terrestrial photogrammetry method in cultural heritage studies: A case study of Seyfeddin Karasungur

Adem Kabadayı, Alperen Erdoğan 62-67

** The use of unmanned aerial vehicle (UAV) data in village development plans: A case study of Aksaray Yaylak Village

Hacı Murat Yılmaz, Nusret Aktan, Adem Çolak, Aydın Alptekin 68-72



Automated measurement of carotid angle with use of CT images

Nusret Demir ^{*1} , Serkan Demir ² 

¹ Akdeniz University, Department of Space Science and Technologies, Antalya, Türkiye

² Medical Sciences University Sancaktepe Research and Application Hospital, Istanbul, Türkiye

Keywords

Medical Image Processing
Photogrammetry
CT
Neurology
Stroke

Research Article

DOI:10.53093/mephoj.1166415

Received: 24.08.2022

Revised: 17.10.2022

Accepted: 19.10.2022

Published:22.12.2022

Abstract

Carotid stenosis is an important etiological factor in the forming of ischemic stroke. The weight of stroke which is formed as a result of extracranial internal carotid artery stenosis or occlusion differs according to the location, size of interaction, collateral supply, and the mechanisms those cause interact. Therefore, it is important to measure the narrowness of the carotid with the calculation of the bifurcation angle. In this study, CT cross-sectional image sequences are used. The images are unsupervised classified, and the carotid veins are identified with the boundaries and centers of the clusters. Then, the angles are calculated with three center points of the veins from successive images. The center point of the calculation is from the vein which has the maximum area difference between one of the successive images. The results are evaluated using 5 samples with visual interpretation regarding the position and the correctness of the three successive images which have maximum area jump.

1. Introduction

There are two types of Carotis Communis vessels that carry blood to the brain: Carotis interna and Carotis externa. The narrowing of the carotid arteries is referred to as carotid artery disease, also known as carotid artery stenosis. In most cases, plaques made of fatty substances and cholesterol are to blame for the carotid's narrowness. The risk of stroke is greatly enhanced if the carotid arteries are occluded. An expanded version of Demir and Demir's study [1] is presented here.

The narrowing of the carotid Interna usually develops after separation from the carotid communities, and the main cause is turbulence flood in this section. Although the death rate has decreased in the recent decade, ischemic paralysis remains a major medical problem. Despite the use of thrombolysis and other treatment options in acute ischemia paralysis, prevention is the most successful approach. The data utilized to determine risk factors are based on epidemiological studies that were conducted at random [2].

As shown in Figure 1, the blood is supplied into the human brain via the right and left internal carotid artery

which is split from the two-sided common carotis artery [3]. The focal neurological situations based on cerebrovascular diseases are called as stroke [4]. Carotis stenosis is an important etiological factor in the forming of ischemic stroke [5]. According to the studies which use Doppler USG, more than 50% of the automatically Carotis stenosis is seen in 4-5% of patients who are elder than 65 years old [6]. The risk of stroke is increased by the degree of stenosis [7].

The weight of a stroke which is formed as a result of extracranial internal carotid artery stenosis or occlusion differs according to the location, size of interaction, collateral supply, and the mechanisms that cause interaction. Stroke causes demoralization and morbidity for the patients [8-10]. Stroke is the third most seen cause of death, and it is the first human disorder [6]. Thus, for detection of narrowness at an early stage has become of high interest to many researchers.

The researches rely mainly on the determination of carotid bifurcation parameters, such as volume, position, etc.

Dix et al. [10] identify the ideal measurement methods and acquisition parameters for CT angiography of carotid bifurcation. They use various measurement

* Corresponding Author

(nusretdemir@akdeniz.edu.tr) ORCID ID 0000-0002-8756-7127
(drsrkndemir@gmail.com) ORCID ID 0000-0003-4395-5141

Cite this article

Demir, N. & Demir, S. (2022). Automated measurement of carotid angle with use of CT images. Mersin Photogrammetry Journal, 4(2), 37-44

approaches to compare SSD images (Shaded surface display), MIP (Maximum Intensity Projection), magnified axial images, and axial images. They offer automation but end with the benefits of CT imaging.

A deformable tubular 3D Non-Uniform Rational B-Splines (NURBS) model is used by Suinesiaputra et al. [11] to design and validate a method for automatic segmentation of the carotid artery lumen from volumetric MR Angiographic (MRA) images. They perform automatic cross-sections from the artery for the carotid measurements using MR imaging with NURBS 3D model output.

Using stereoscopic PIV (Particle Image Velocimetry) measurements, Kefayati and Poeping [12] describe the disrupted flow in the stenosed carotid artery.

Fisher [13] investigates the effect of the geometry of carotid arteries into the flow characteristics. He shows that the apoptotic and biochemical changes of upstream carotid plaque are closely linked to the development of stroke symptoms. Similarly, Stroud et.al [14] perform a numerical analysis of flow through a severe stenosis carotid artery bifurcation to investigate the geometry of the vessels.

There is research that computes the blood flow in the vessels using numerical models.

Cebral et al. [15] created a technique for creating accurate patient-specific finite element models of carotid artery blood flow. With a tubular deformable model along each artery branch, they used MR data to build anatomical models. At two points below and above the bifurcation, they calculated the flow velocities. They made it possible to describe the created model's flow patterns.

Tan et al. [16] develop turbulence models to predict blood flow patterns in the carotid artery and calculate the oscillating vessel Wall stresses. The model is MR image-based and simulated the wall shear stress.

In order to determine the mechanical properties resulting from the influence of the lipid core and calcification within a plaque, Wong et. al. [17] design a numerical simulation that reflects the distribution and structure of plaque via 3D blood-vessel modeling.

Gul and Bernhard [18] applied three methods for modeling pressure and flow in carotid bifurcation. They investigate the model parameters such as flow resistance, diameter, and length of the vessel.

Klooster et. al. [19] developed a method to register MR images to allow the classification of the vessel walls to investigate the plaque components.

Using computational fluid dynamics (CFD) with single-layer and multilayer models, Lawrence-Brown et. al. [20] explore the biomechanical stress and strain behavior within the wall of the artery and its impact on plaque formation and rupture. They ran a CFD analysis to display the wall shear pressure and stress.

Cross sectional CT imaging is used by McNamara et. al. [21] to identify patients with a high carotid bifurcation who may be more likely to experience surgical problems. Since their methodology relies on hand measurements, the outcomes could vary depending on the measurements used.

The methods mentioned above are highly depending on the calculation of position e.g., volume and blood flow

estimation in the carotid bifurcation. On the other hand, our research focuses the measurement of the narrowness with calculation of the angle automatically.

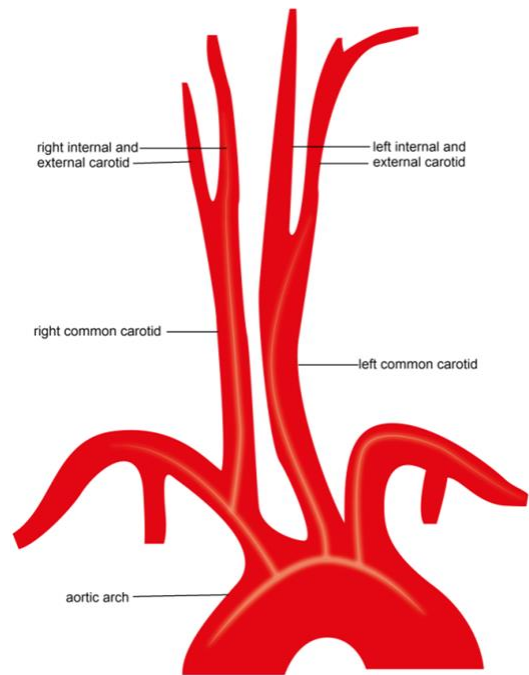


Figure 1. Carotid artery

2. Method

Cross-sectional CT imagery is used for this work. A random number of image samples is provided for each patient. The images are acquired as a cross-section in every 0.5 mm. CT images are gray-scale, and carotid vessels are visually separable from the image background, which allows running the traditional image classification methods such as ISODATA [22].

The processing chain starts with image classification. The classification approach segments the image into different categories which include the carotid vein clusters. Then, the process is followed by morphological erosion to overcome the connectivity problem of the separated veins in the images although they are separate in reality. Then, the distances between the center and the created points along the cluster boundaries are calculated to determine the circularity of the cluster.

Three parameters are used to determine the cluster if it belongs to the carotid vein class; the standard deviation of the distance values between the center and boundary points; the minimum and maximum vein section size; the maximum distance between the center points which come from the images. If three criteria meet the defined thresholds, then the corresponding cluster is selected as a carotid vein.

The areas are compared between the clusters from the successive images. The cluster which shows the maximum area difference among all the pairs is selected as the bifurcation part of the carotid. The angle is calculated between the selected vein center point and the center points from one image before and after. The processing schema can be found in Figure 2.

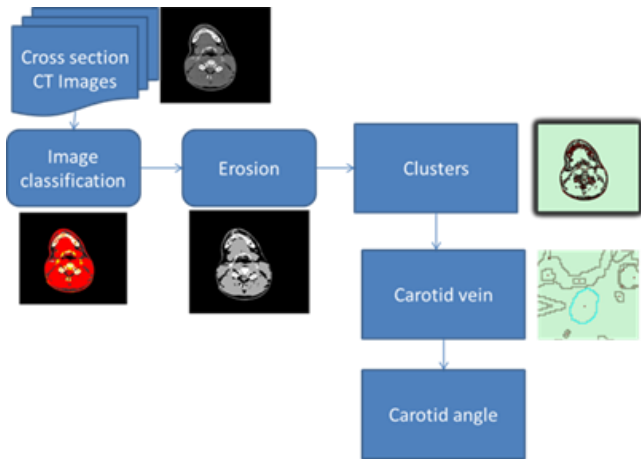


Figure 2. Processing workflow

2.1. CT Image classification

Image classification methods are widely used in urban planning, mapping applications, extraterrestrial research, forensic applications, medical image analysis, and many other topics which use imagery information. It is a technique that classifies image pixels into different categories. In medical image analysis, these categories can be listed as vessels, the brain, and other parts of the imaged part of the body.

The first step of image classification is the identification of the feature parameters with spectral characteristics. Then, feature space is divided into subspaces which do not overlap between each other. The classification is finalized with the calculation of the distance between image pixels and each subspace.

There are two types of image classification, one is unsupervised and the other is supervised image classification. In supervised classification, prior knowledge is used to determine the membership of pixels to the corresponding classes. The user selects the pixels with his own knowledge, and the algorithm estimates the parameters with this prior knowledge. There are several algorithms that are used for supervised classification. One uses a minimum distance to assign the pixel to the corresponding class. In this algorithm, the minimum distance is computed between the center of the class and the pixel value. The center of the class is calculated using the training pixel samples.

Another algorithm is maximum likelihood classification which calculates the likelihood of each pixel point by point and assigns the pixel to the corresponding class with the maximum likelihood. Maximum likelihood classification (MLC) is one of the most widely used techniques in supervised classification. Other supervised classification methods are Parallelepiped classification and Decision tree classification. Parallelepiped classification is based on a single rule while the decision tree considers different characteristics of the objects.

The unsupervised classification does not use any of the existing prior knowledge and creates clusters from the image according to its spectral characteristics. There are two kinds of unsupervised classification which are mostly used in many image processing applications which are K-means and ISODATA classification.

Both have two different aspects. K-means adjust a class each time, and each class's average value is

recalculated. ISODATA recalculates the class averages after adjusting all samples. Both are standard classification methods in any remote sensing software package.

The classical ISODATA classification algorithm has the following steps; first, the average gray value of the whole image is calculated. Secondly, the image is classified using the calculated average as the threshold value. Then, the average values are calculated for the created classes, and these values are used as new thresholds. This is repeated unless the threshold values are not changed anymore.

CT images are in gray scale, and the carotid vessels might be imaged from different directions. On the other hand, carotid vessels are separable from another background in the images also visually (Figure 3).



Figure 3. Original CT image of the bifurcation position

Finding the different vessel classes on the images is the first challenge. In its most basic form, CT imagery is grayscale. In comparison to other areas of the photos, the vessels are noticeably brighter. Using image classification methods like the ISODATA algorithm, this information is adequate to identify carotid vessels.

A collection of samples are grouped using the clustering algorithm used by ISODATA, and each sample is represented as a vector, such as $X=[x^1, \dots, x^N]^T$. The cluster is automatically updated after each iteration to combine comparable segments and to break segments with high standard deviations. The following equation is used to determine the sum of squared distances between each pixel and its associated cluster center:

$$SS_{distances} = \sum (X - C(x))^2 \quad (1)$$

where $C(x)$ is the cluster mean for the pixel x . The Mean Squared Error (MSE), which is calculated as follows, is used to identify cluster variability.

$$MSE = SS_{distances} / (N - c) \quad (2)$$

where N is the number of pixels, c indicates the number of clusters, and b is the number of spectral bands, for CT images it is 1 [1,22].

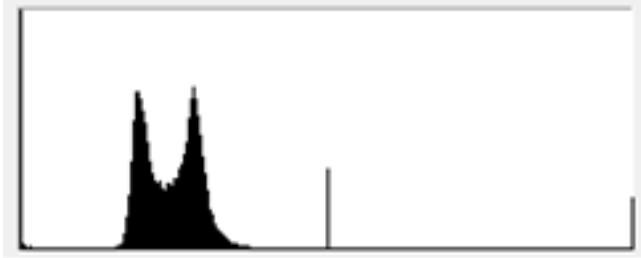


Figure 4. Histogram of CT image

As shown in Figure 4, five classes are defined with analysis of the number of peak points over the histogram. Figure 5 shows the classification result.

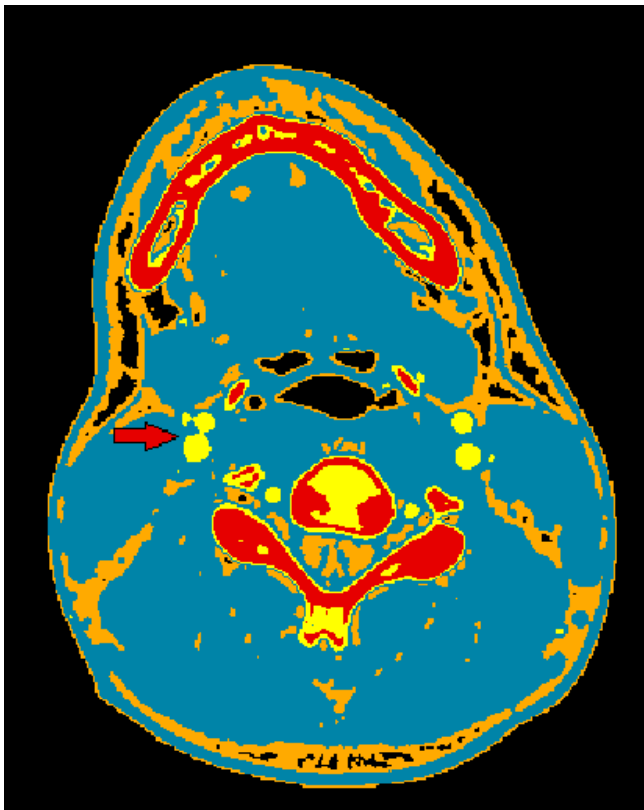


Figure 5. Classified CT image, the colors represent different clusters

2.2. Morphological operation

After clustering each section image, morphology operator erosion has been applied to the classification result to identify the vessels which are separated in reality but look connected to the images.

Morphological operations are one of the basic processes in image processing, and they apply a structuring element over the input image and create an output image. The pixel values of the input image are compared with the neighbors; the size and shape of the neighbors directly affect the result of the operations. Since the centers are the point of interest, not the boundaries, erosion is only the used approach. Erosion removes the pixels on the object boundaries by removing a number of pixels from the objects in the input image.

As seen in Figure 6, the carotid vessels are separated using erosion since the connectivity of the veins is caused by image artifacts.

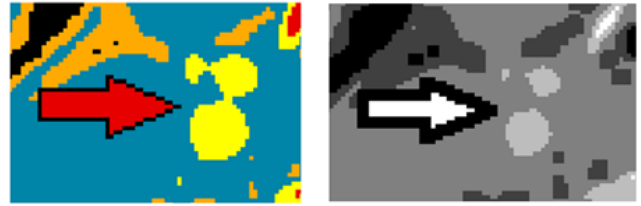


Figure 6. Before (left) and after(right) morphological operation

2.3. Identification of the carotid veins

The main idea to identify the vein clusters is using the standard deviation of the distance series between the cluster center and the vein boundary. Secondly, the veins have a certain size compared to the other clusters.

The vessels that part of the carotid artery have a circular form. The circularity can be determined with statistical analysis by calculating the standard deviation of the distance between the center and the border of the vessels. To do this, the centers of vessel clusters have been extracted, and then a series of vessel border points is generated. The distance is calculated between each border point and the center point. The center and boundary points are created using the ArcGIS software package (Figure 7). It simply extracts the centroid of the clusters and creates the points along the cluster boundaries. The gap between the points is set as a ground sample distance value.

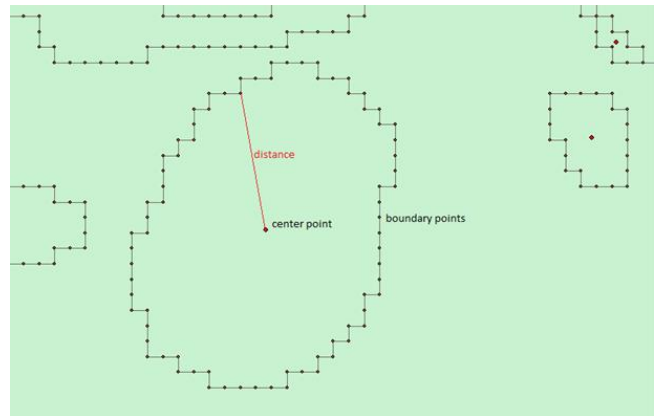


Figure 7. The center and boundary points of the extracted classes

The distance between the cluster and the boundary point is calculated as follows;

$$D_i = \sqrt{(X_c - X_{ib})^2 + (Y_c - Y_{ib})^2} \quad (3)$$

$$s^2 = \frac{1}{n-1} \sum_{i=1}^n (D_i - \bar{D})^2 \quad (4)$$

X_c, Y_c values are coordinates of the center point, X_b and Y_b values are the coordinates of the boundary point i , D_i is the calculated distance with i th boundary point, s^2 is variance, \bar{D} is the mean value of all distances, n number of calculated distance value.

Another criterion is the area of the clusters. The maximum and minimum area thresholds are set by consideration of vein geometry.

The center points of the clusters which meet certain criteria (circularity and area) are overlaid and the distances of the center points are calculated between each other. The carotid center points always remain and they should be in a certain distance between each other after overlaying altogether on the same plane. The number of center points which are close each other is same as the number of the used image.

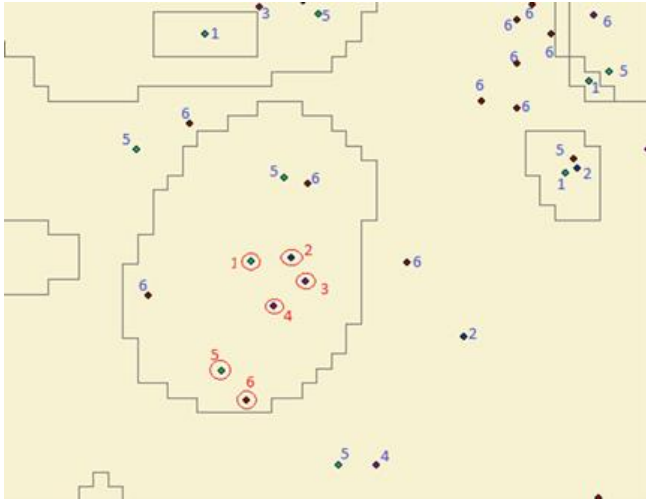


Figure 8. The image numbers of the overlaid center points

As shown in Figure 8, the center points of clusters are overlaid on the clusters image from image 1. Each point has the number of its image label.

The process starts with the first image,

- Takes the center points,
- Then check if there is any center point in its neighborhood from the next image, here image 2.
- If any point is found, then the next center point from the next image is searched in the neighborhood of the center point from the successive images.
- This process is continued until the last image.

In the Figure 8, each cluster centers are numbered with their image numbers. The number of neighbor points is same as the number of used images. This case is valid only for the carotid veins (red points in Figure 8).

2.4. Calculation of the angle

Three center points are used to calculate the carotid angle, one center point in the middle and the other two center points from the images before and after. The center point which is in the middle is selected based on the area difference between clusters. The vein cluster which has the biggest area difference between the clusters from the image after is selected as the middle, and its center point is the used center point for the angle calculation.

Let PC [1...n] center points from the same cluster from successive images. PC_i is the cluster in the middle, which is the bifurcation area of the vein. PC_{i-1} and PC_{i+1} successive point those used in the angle calculation.

PC_i, PC_{i-1}, and PC_{i+1} are the center points from the selected clusters for calculating the angle as shown in Figure 9.

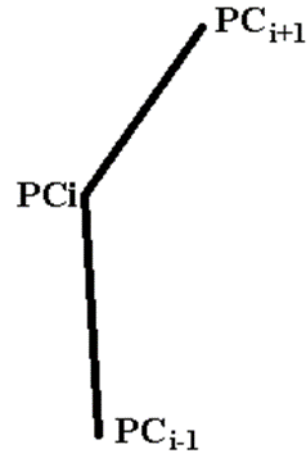


Figure 9. Illustration of carotid vein center points

The angle θ is calculated using following formulas;

$$\overrightarrow{PC_{i+1}PC_i} = PC_{i+1} - PC_i \quad (5)$$

$$\overrightarrow{PC_iPC_{i-1}} = PC_i - PC_{i-1} \quad (6)$$

$$\overrightarrow{PC_{i+1}PC_i} \cdot \overrightarrow{PC_iPC_{i-1}} = \|\overrightarrow{PC_{i+1}PC_i}\| \cdot \|\overrightarrow{PC_iPC_{i-1}}\| \cdot \cos \theta \quad (7)$$

$$\theta = \arccos \left(\frac{\overrightarrow{PC_{i+1}PC_i} \cdot \overrightarrow{PC_iPC_{i-1}}}{\|\overrightarrow{PC_{i+1}PC_i}\| \cdot \|\overrightarrow{PC_iPC_{i-1}}\|} \right) \quad (8)$$

From the image acquisition, the Z difference between each image is 0.5 mm. Z coordinate is set as 0 for the center points at the image in the bottom, other center points from the successive images have Z coordinate according to image position in the acquisition (e.g., Z coordinate for the 4th image would be 0.05 x 4 = 0.2 mm).

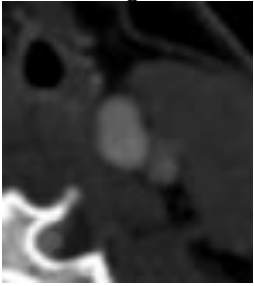
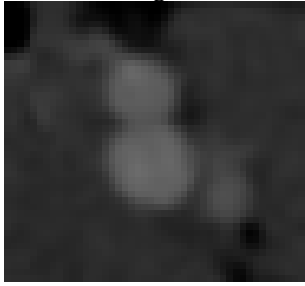


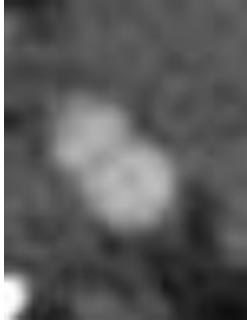



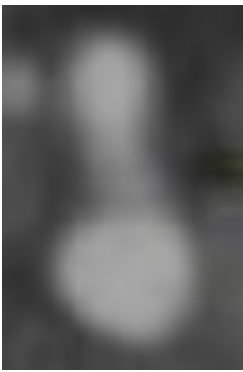


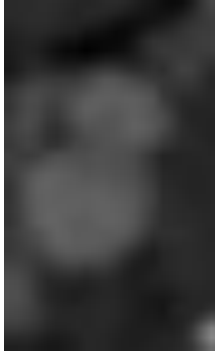



3. Results

For testing the method, 15 crosses sectional CT images from 5 different patients are used. After image classification, erosion is applied on the extracted clusters for each cross-sectional CT image.

The center and boundary points are extracted to analyze the carotid vein clusters.

Table 1 shows the three images which have been used in the angle calculation from the output of the method and the calculated angles. On the other hand, the information regarding the position of the carotid is also achieved depending on the coordinates of the angle with respect to the image center.

Table 1. Quality evaluation of the results, only three clipped images which shows the case of bifurcation

Image 1	Image 2	Image 3	Angle (Degrees)	Position
			38.6823	Right
			43.5219	Right
			30.2174	Right
			12.1425	Left
			54.1151	Right

The results are evaluated with a visual interpretation of three image outputs from the tests. In case three images are the ones that have a bifurcation in the middle, then the result from the method has been confirmed. According to the performance evaluation, for all the tested image samples, the developed method gave the correct three images, including the bifurcation point in the middle, including giving information about the side of the carotid angle.

4. Discussion

The measurement of a carotid angle is often performed with manual measurements on the CT images by medical doctors. Even one-pixel movement during the measurement, may shift the value of the angle, therefore some methods have to be developed accordingly to allow precise measurement.

Cross-sectional CT images are used in previous studies [21]. McNamara et.al [21] used an external software to measure the carotid artery and straight-line distance to identify the high carotid bifurcation. Their measurement is performed with use of the base of skull. On the other hand, there are studies which are based on simulating blood flow in the veins [21]. Lawrence-Brown analyzes stress in carotid artery [20]. Our method uses cross sections of carotid artery which makes it different than the other methods since they derive the angle values with manual measurements on the acquired images. The evaluation is difficult since it is only possible with manual measurements, but it will be meaningless in case the calculated angles would be compared with the ones which derived on the images manually. Therefore, the only evaluation could be done with checking their position right or left. If the image coordinates of the carotid stay on the left of the image center, then the carotid was classified as left, else right.

5. Conclusion

The narrowness of carotid angle is an important factor for the human health. In general, the carotid angle is calculated with manual measurements by the medical doctors. In this study, a new method is developed to calculate the carotid angle using cross sectional CT images.

Our method automatically select the image where the bifurcation occurs, and then calculates the angle between three images, the image with a bifurcation in the middle, and one image after and other before the bifurcation.

The evaluation shows that the selected images are all correct for the calculation of the carotid angle. This allows medical doctors to select the image which has bifurcation without any mistake, and to have the carotid angle without performing any manual measurement with better accuracy.

Future work may include the reconstruction of the carotid vein to allow analyzing the blood flow in the carotid veins in 3D, the analyzing of the role of the carotid communis on the patients with stenosis.

Acknowledgement

We would like to thank to Dr. Cahit Kafadar for his support for data acquisition, and artist Nuray Ergindir Kucukkaya for her support for the artwork of [Figure 1](#).

Author contributions

Nusret Demir: Conceptualization, Methodology, Data curation, Writing-Original draft preparation, Software, Validation. **Serkan Demir:** Visualization, Investigation, Writing-Reviewing and Editing.

Conflicts of interest

The authors declare no conflicts of interest.

References

- Demir, N., & Demir, S. (2015, May). Automated calculation of bifurcation carotid angle for analyzing the risk of carotis plaques by using carotid CT angiographic images. In *Smart Biomedical and Physiological Sensor Technology XII* (Vol. 9487, pp. 91-99). SPIE.
- Midi, İ., & Afşar, N. (2010). İnme risk faktörleri. *Klinik Gelişim*, 10(1), 1-14.
- Bouthillier, A., Van Loveren, H. R., & Keller, J. T. (1996). Segments of the internal carotid artery: a new classification. *Neurosurgery*, 38(3), 425-433.
- Adams, R. D., Victor, M., Ropper, A. H., & Daroff, R. B. (1997, July). Principles of neurology. *Neuropsychiatry, Neuropsychology & Behavioral Neurology*, 10(3), 220
- Autret, A., Saudeau, D., Bertrand, P. H., Pourcelot, L., Marchal, C., & De Boisvilliers, S. (1987). Stroke risk in patients with carotid stenosis. *The Lancet*, 329(8538), 888-890.
- Inzitari, D., Eliasziw, M., Gates, P., Sharpe, B. L., Chan, R. K., Meldrum, H. E., & Barnett, H. J. (2000). The causes and risk of stroke in patients with asymptomatic internal-carotid-artery stenosis. *New England Journal of Medicine*, 342(23), 1693-1701.
- Ringelstein, E. B., Koschorke, S., Holling, A., Thron, A., Lambertz, H., & Minale, C. (1989). Computed tomographic patterns of proven embolic brain infarctions. *Annals of Neurology: Official Journal of the American Neurological Association and the Child Neurology Society*, 26(6), 759-765.
- European Carotid Surgery Trialists Collaborative Group. (1991). MRC European Carotid Surgery Trial: interim results for symptomatic patients with severe (70-99%) or mild (0-29%) carotid stenosis. *Lancet*, 337, 1235-1243.
- Mayberg, M. R., & Winn, H. R. (1995). Endarterectomy for asymptomatic carotid artery stenosis: resolving the controversy. *JAMA*, 273(18), 1459-1461.
- Dix, J. E., Evans, A. J., Kallmes, D. F., Sobel, A. H., & Phillips, C. D. (1997). Accuracy and precision of CT angiography in a model of carotid artery bifurcation stenosis. *American journal of neuroradiology*, 18(3), 409-415.

11. Suinesiaputra, A., de Koning, P. J., Zudilova-Seinstra, E., Reiber, J. H., & van der Geest, R. J. (2012). Automated quantification of carotid artery stenosis on contrast-enhanced MRA data using a deformable vascular tube model. *The International Journal of Cardiovascular Imaging*, 28(6), 1513-1524.
12. Kefayati, S., & Poepping, T. L. (2010, January). 3-D flow characterization and shear stress in a stenosed carotid artery bifurcation model using stereoscopic PIV technique. In *2010 Annual International Conference of the IEEE Engineering in Medicine and Biology* (pp. 3386-3389). IEEE.
13. Fisher, M. (2012). Geometry is destiny for carotid atherosclerotic plaques. *Nature Reviews Neurology*, 8(3), 127-129.
14. Stroud, J. S., Berger, S. A., & Saloner, D. (2002). Numerical analysis of flow through a severely stenotic carotid artery bifurcation. *Journal of Biomechanical Engineering*, 124(1), 9-20.
15. Cebal, J. R., Yim, P. J., Löhner, R., Soto, O., & Choyke, P. L. (2002). Blood flow modeling in carotid arteries with computational fluid dynamics and MR imaging. *Academic radiology*, 9(11), 1286-1299.
16. Tan, F. P. P., Soloperto, G., Bashford, S., Wood, N. B., Thom, S., Hughes, A., & Xu, X. Y. (2008). Analysis of flow disturbance in a stenosed carotid artery bifurcation using two-equation transitional and turbulence models. *Journal of biomechanical engineering*, 130(6), 061008
17. Wong, K. K., Thavornpattanapong, P., Cheung, S. C., Sun, Z., & Tu, J. (2012). Effect of calcification on the mechanical stability of plaque based on a three-dimensional carotid bifurcation model. *BMC cardiovascular disorders*, 12(1), 1-18.
18. Gul, R., & Bernhard, S. (2015). Parametric uncertainty and global sensitivity analysis in a model of the carotid bifurcation: Identification and ranking of most sensitive model parameters. *Mathematical biosciences*, 269, 104-116.
19. van 't Klooster, R., Staring, M., Klein, S., Kwee, R. M., Kooi, M. E., Reiber, J. H., ... & van der Geest, R. J. (2013). Automated registration of multispectral MR vessel wall images of the carotid artery. *Medical physics*, 40(12), 121904.
20. Lawrence-Brown, M., Stanley, B. M., Sun, Z., Semmens, J. B., & Liffman, K. (2011). Stress and strain behaviour modelling of the carotid bifurcation. *ANZ Journal of Surgery*, 81(11), 810-816.
21. McNamara, J. R., Fulton, G. J., & Manning, B. J. (2015). Three-dimensional computed tomographic reconstruction of the carotid artery: identifying high bifurcation. *European Journal of Vascular and Endovascular Surgery*, 49(2), 147-153.
22. Ridler, T. W., & Calvard, S. (1978). Picture thresholding using an iterative selection method. *IEEE trans syst Man Cybern*, 8(8), 630-632.



© Author(s) 2022. This work is distributed under <https://creativecommons.org/licenses/by-sa/4.0/>



Use of unmanned aerial vehicle (UAV) for mapping, and accuracy assessment of the orthophoto with and without using GCPs: A case study in Nepal

Abinash Silwal ^{*1}, Sunil Tamang ¹, Rajendra Adhikari ²

¹Kathmandu University, Department of Geomatics Engineering, Dhulikhel, Nepal

²Kathmandu University, Department of Physics, Dhulikhel, Nepal

Keywords

Photogrammetry
UAV
GIS
Orthophoto
HPC

Research Article

DOI:10.53093/mephoj.1176847

Received: 18.09.2022

Revised: 20.10.2022

Accepted: 09.11.2022

Published: 22.12.2022

Abstract

The conventional methods of aerial photogrammetry using helicopters or airplanes are costly and challenging for small areas. For a developing country like Nepal, where Geospatial data is in high demand, a new competitive approach is essential for rapid spatial data acquisition at a low cost and time. This article demonstrates how this can be achieved using one of the evolving remote sensing technology, Unmanned Aerial Vehicles (UAVs). The application of UAVs is rapidly increasing in Nepal due to its capability of acquiring images remotely and the potential to provide data with a very high spatial and temporal resolution even in inaccessible terrain at a relatively low cost. Here, the performance of UAVs for topographical surveying and mapping has been investigated, along with the comparison between orthophoto obtained using GCPs, and without using GCPs. For this study, a DJI Phantom 3 Advanced quadcopter collected about 700 images at a flying height of 50 m above the settlement area. An orthophoto of 3.78 cm GSD covering 40.83 hectares of area was produced. With appropriate ground control points, an absolute positional accuracy of 0.035 m RMSE was achieved, whereas the output obtained without using GCPs was satisfactory. This study also highlights the use of a High-Performance Computing (HPC) system and open-source platform for rapid image processing.

1. Introduction

Geospatial data and spatially aware technologies play a crucial role in infrastructure planning and development in every country [1]. Almost all the sectors of a nation have a spatial component, from cadastral records, land use, land cover, and smart cities to utility lines, transportation networks, and critical infrastructure [2]. There is an urgent need to change Nepal's development model because its current development path is not aiding it to escape from the low-growth trap it is in [3]. So, the country's development model should be reformed. Geospatial technologies can revolutionize a country's economy by assisting effective planning of infrastructure and sustainable development [4-5].

Unmanned Aerial Vehicle in the surveying industry is a new competitive and affordable approach for countries like Nepal for rapid spatial data collection at less cost and time [6-7]. The application of UAVs is rapidly increasing in Nepal due to its capability of

acquiring images remotely and the potential to provide data with a very high spatial and temporal resolution even in inaccessible terrain at a relatively low cost [7-9].

UAV, also known as a drone, is an aircraft that can fly without a pilot [10-11]. It can fly autonomously and can be either human-operated or self-programmed in a wide range of missions that can be controlled from a ground base station [12]. It is a controllable platform for the data collection process that can go through risky areas to collect information rapidly and update the data without delay like satellite images or terrestrial surveying [13-15]. Aerial photogrammetry with aircraft is expensive and hard to operate with sophisticated planning. So, UAVs have become adequate and preferable among surveyors [16-17].

UAV use in research has increased over the past decades, which has greatly increased their significance [18-19]. This is further supported by the volume of academic articles on UAVs that have been published in various research communities during the past 20 years.

* Corresponding Author

^{*}(afactor.abinash@gmail.com) ORCID ID 0000-0002-2285-4643
(tamangsunil112233@gmail.com) ORCID ID 0000-0002-0295-9632
(rajendra.adhikari@ku.edu.np) ORCID ID 0000-0001-6649-7097

Cite this article

Silwal, A., Tamang, S., & Adhikari, R. (2022). Use of unmanned aerial vehicle (UAV) for mapping, and accuracy assessment of the orthophoto with and without using GCPs: A case study in Nepal. *Mersin Photogrammetry Journal*, 4(2), 45-52

According to [18], since then, more than 80,000 articles featuring the terms "UAV" or "drone" in the title or the keywords have been published, with the bulk of these works falling under the engineering and computer science fields and the majority of contributions coming from remote sensing domain [18, 20]. This technology has been effectively used for ecological applications [21-24], glacier monitoring [25], natural disasters [11, 17, 26], agriculture surveillance [27-29], and other environments that are continually changing [7, 30-33].

The accuracy of UAVs for land surveying and mapping has been demonstrated all around the world. In Taiwan, for instance, [34] examined high-accuracy topographic mapping using UAV-based images and determined the integration capability of topographic maps via the image of UAV and GCPs. According to [34], UAV-based surveying may eventually be an effective replacement for GPS and total stations. Working on the application of UAV in Ghana for topographical mapping of inaccessible land, [35] concluded that, for mapping inaccessible locations, the combination of RTK technology with UAV and GIS is a viable and adequately accurate option and also recommends it for the creation of precise geometry and cross-sectional drawings for the design of Tailings Storage Facility (TSF).

Likewise, this study also investigates the performance of UAV for topographical mapping and compares the accuracy with and without using GCPs. This study involves image acquisition using UAV, Ground Control Points (GCPs), and check Points (CPs) establishment using DGPS, image processing using HPC, accuracy assessment, and finally extraction of 2D features and analysis using open-source GIS software.

2. Study Area

A study area is located around the Kathmandu University Central Campus, Kavre District, Bagmati Province, Nepal. It is shown in Figure 1. The total area of this site is about 40 hectares. The elevation of the site ranges from about 1400m to 1480m above the mean sea level. This area includes built-up areas, open spaces, water bodies, road networks, and agricultural land - so it was chosen.

3. Material And Methods

For this study, DJI Phantom 3 Advanced quadcopter with the following specification was used. Table 1 depicts the specification of the UAV used in this study.

A schematic overview of the methodology workflow is shown in Figure 2.

Table 1. Specification of UAV (DJI Phantom 3 Advanced)

Model	DJI Phantom3 Advanced
Camera	FC300S
Resolution	12.4 MP
Sensor width and height	6.317 [mm] x 4.738 [mm]
Image Size (max.)	4000 X 3000
Pixel Size	1.56*1.56 μm
Focal length	3.6 mm
Geolocation	On-board GPS
Control System	Remote/phone/table

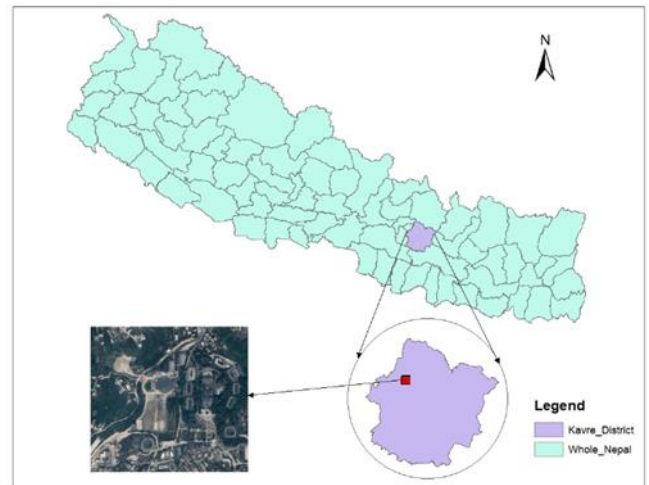


Figure 1. Study Area Map

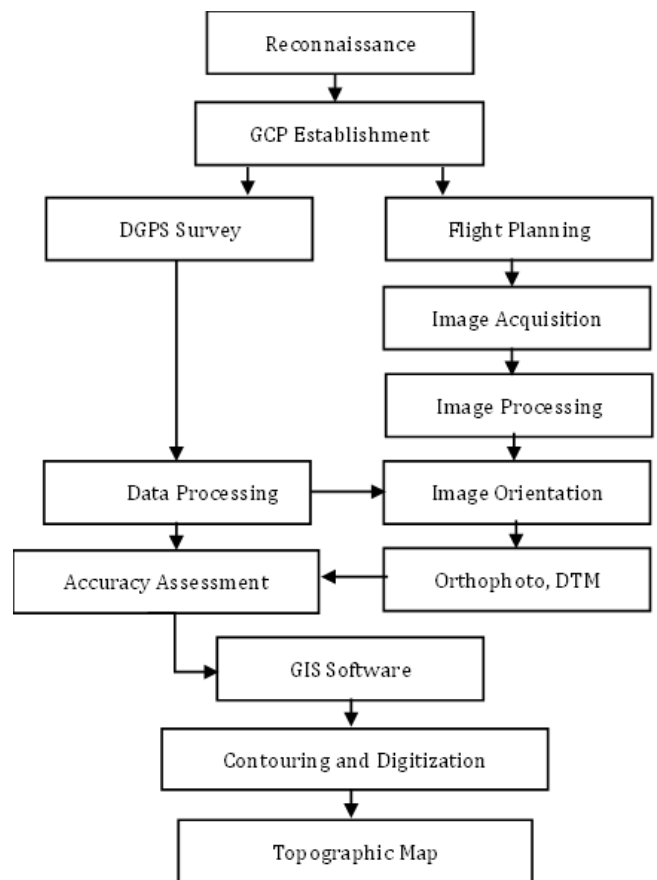


Figure 2. The workflow of methodology

3.1. Reconnaissance

At first, a desk study was done by looking at Google maps and existing Topographical maps of the study area, and necessary planning and preparation were done.

3.2. GCP Establishment

The GCPs and CPs were established for georeferencing and accuracy assessment, respectively. A total of 14 points were installed on the ground. The GCPs and CPs were selected considering the proper distribution in all the parts of the study area and clear

aerial visibility. GCP and CP were established by static DGPS method using a GNSS receiver [36].

3.3. Flight Planning and Image Acquisition

Flight planning was done using the Pix4D capture application above the study area. The UAV flew autonomously in a pre-defined flight plan at an approximate altitude of 50m above ground. Several UAS criteria as mentioned by [37] were considered while choosing flight parameters. A total of 700 geotagged images were taken from a nadir perspective, with 80% forward and 70 % side overlap. Although percentages of forward and side overlaps vary depending on the kind of terrain [38], the research on UAV imagery acquisition suggests above 70% forward and 60–70% side overlap for the majority of situations [39-40].

3.4. Image Processing

Images captured from UAV were processed in Pix4D mapper and Web Open Drone Map (ODM) - in the HPC system, also known as Supercomputer. WebODM is an open-source platform written in the Python programming language designed to perform photogrammetric analysis and processing of UAV imagery [41]. Image processing involves several steps which are discussed in the later part.

3.5. Image Orientation

Image orientation was done using 14 high-accuracy ground control points (GCPs). Figure 3 shows the 14 points statically surveyed on the ground using DGPS/GNSS receiver with approximately 1.8 cm standard deviation. These points were marked using a notable flag during image acquisition. Out of the 14 points, seven were selected as GCP for the exterior orientation process, and seven were considered CP for accuracy assessment. It was ensured that each point got marked in at least six images to avoid distortion [36].

Similarly, images were also oriented without using the ground control points to test the accuracy with UAV onboard GPS. It can help to quantify the geolocation differences when it is not possible to collect GCPs. All GCPs were assigned to be checkpoints for checking the accuracy of this output.

3.6. Dense point cloud generation

After a proper internal and external orientation, a dense matching technique was applied to represent the object space through dense point clouds. These point clouds are, later on, structured, interpolated, simplified, and textured for photo-realistic representation and visualization [42]. To generate a mesh and create a surface with all the terrain features, it is used directly [33].

3.7. Orthophoto Generation

After interpolating the 3D points generated in previous steps, a triangulated irregular network was formed, which resulted in a Digital Surface Model (DSM). Now, to develop an orthophoto, the orthorectification process was performed from DSM. This task produced an orthogonal projection from the initially taken images by re-projecting the original image pixels [23]. Moreover, to retrieve a more appealing orthophoto, texture and color balancing were applied.

3.8. Accuracy Assessment

Quantitative accuracy assessment was done using CPs. Root Mean Square Error (RMSE) result is used to display the accuracy value of the dataset by calculating the difference between reference and observed coordinates [36, 40]. On the other hand, the features' appearance in the orthophoto, deformations, and hazes were checked through visual inspection for qualitative evaluation. Also, the positional accuracy of orthophoto obtained using GCPs and without GCPs was compared. It helped to know the accuracy and their corresponding application in each condition.

3.9. Map Preparation

After getting a true orthophoto, all the spatial data are extracted by digitizing it in GIS software. Similarly, the contour is also generated using Digital Terrain Model (DTM). Due to the high-resolution orthophoto, even small features and changes were detected. Finally, they are combined to prepare a topographical map.

4. Results and Discussion

4.1. Coordinates Collected

The processed coordinates that were obtained from raw data after the GNSS survey are shown below. Table 2 shows the coordinates of GCPs, which were used to georeference the images, whereas Table 3 represents the coordinates of CPs used for the accuracy assessment of the orthophoto.

Table 2. Ground Control Point Coordinates

GCP Name	Easting (m)	Northing (m)	Elevation (m)
1000	355785.301	3055784.53	1459.631
1001	355737.436	3056024.12	1443.244
1003	355435.732	3055657.31	1418.243
1013	355883.056	3055904.63	1451.323
1008	355556.938	3055921.53	1418.751
1012	355800.501	3055885.7	1466.698
1015	355893.612	3055677.96	1448.762

Table 3. Check Point Coordinates

CP Name	Easting (m)	Northing(m)	Elevation(m)
1004	355588.556	3055682.47	1442.044
1006	355688.922	3055794.37	1430.637
1007	355760.222	3055735.94	1445.875
1009	355737.705	3055913.09	1451.685
1010	355771.695	3055947.9	1457.136
1011	355812.974	3055966.78	1451.311
1014	355905.762	3055756.41	1438.522

4.2. Image Orientation

For image orientation, two experiments were carried out. One was Georeferencing using ground control points, and the other was orientation using geotags images only, without relying on ground control points.

Geolocation results (errors in x, y, and z) using GCPs and Check Points are shown in Table 4 and Table 5, respectively. While using GCPs, the model is geolocated accurately with an accuracy of 4 cm in x, 2 cm in y, and 3 cm in z. It is a significantly high accuracy, which can be used for any project.

Table 4. Geolocation result with GCPs

GCP Name	Error X [m]	Error Y [m]	Error Z [m]
1000	-0.095	0.033	0.047
1012	-0.0106	0.0053	0.0405
1003	0.001	0.002	-0.005
1008	0.004	-0.002	-0.006
1001	-0.032	-0.049	0.057
1015	0.028	0.009	-0.009
1013	0.072	-0.03	-0.014
Mean[m]	-0.00466	-0.00453	0.01579
Sigma[m]	0.04780	0.02497	0.02851
RMSE(m)	0.04493	0.02374	0.03049

Table 5. Check Point Errors

CP Name	Error X [m]	Error Y [m]	Error Z [m]
1004	-0.06385	0.0804	-0.0224
1006	-0.03139	0.039	-0.1065
1010	-0.0361	-0.0467	0.0871
1011	0.0253	-0.0565	0.0883
1007	-0.0544	0.0512	-0.0446
1014	0.0204	-0.0443	-0.0423
1009	-0.0579	-0.0402	-0.0591
Mean [m]	-0.02828	-0.002443	-0.01421
Sigma[m]	0.034093	0.052802	0.068748
RMSE[m]	0.044293	0.052859	0.070202

In another case, the images were processed in WebODM without using GCPs. Images were oriented with geotags only using the HPC system, which resulted, in a speedy orthophoto generation. The geolocation check result is shown in Table 6. The result is relatively less accurate, especially in the case of height. It is due to only the use of inbuilt GPS that is present in UAV. However, this result is promising for projects that require an accuracy of less than a meter. The limited accuracy is because of not using ground control points, GPS quality, and lack of precise time synchronization between the image acquisition and GPS receiver.

Table 6. Geolocation results without GCP

CP Name	Error X [m]	Error Y [m]	ErrorZ [m]
1004	-0.4155	0.3985	-0.5242
1006	-0.1148	0.1039	-0.4556
1010	-0.3067	-0.41457	0.6081
1011	0.1983	-0.2085	0.7738
1007	-0.2595	0.31921	-0.9954
1014	0.46027	-0.20344	-0.8423
1009	-0.20779	-0.18012	-0.6591
Mean [m]	-0.09225	-0.02643	-0.29924
Sigma[m]	0.288347	0.281773	0.650142
RMSE[m]	0.302743	0.283010	0.715703

4.3. Orthophoto

Finally, the orthophoto with 3.78 cm/pixel resolution was produced as shown in Figure 3. The quality of the orthophoto is outstanding as all the objects have been orthorectified, and the features can be detected very clearly.

This orthophoto can be a reliable source for digitization, feature extraction, various map preparation, and other spatial planning activities. Digital Surface Model (DSM) can also be seen in Figure 4, which has been extracted from orthophoto. The elevation of DSM ranges from 1402.45 m to 1481.75m.



Figure 3. Orthophoto of Study Area

4.4. Accuracy Assessment

Checkpoints were used to analyze the quantitative accuracy of the model. As shown in Table 5, while using GCPs, the Root Mean Square Error (RMSE) in X, Y, and Z were 4 cm, 5 cm, and 7 cm, respectively. Similarly, while GCPs were not considered, as shown in Table 6, RMSE in X, Y, and Z were 30cm, 28cm, and 71cm, respectively. The result obtained using GPC is excellent and can be used for high-precision works. Previous studies, for example, done by [36, 43, 44] have given average RMSE of ± 0.05 m, ± 0.338 m, and ± 0.283 m respectively for planimetry and ± 0.300 m, ± 0.704 m, and ± 0.178 m respectively for height. The accuracy result shown by this study is more promising.

On the other hand, the vertical error without ground control points is comparatively high because of the consumer-grade inbuilt GPS of UAV. This error is a bit high but can be helpful in mapping works that don't require absolute accuracy. UAVs may often be used for emergency mapping applications in areas where human accessibility is hard, and it's not easy to take GCPs; in such cases, this result shows the accuracy will be promising. However, a highly accurate model using GCP was used to get the final output for this study.

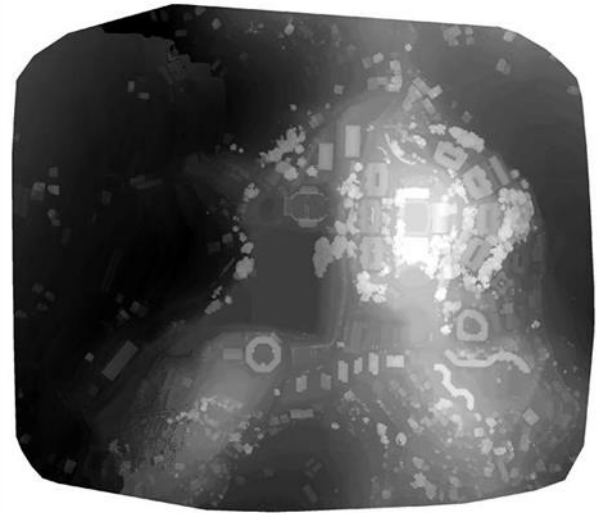


Figure 4. Digital Surface Model

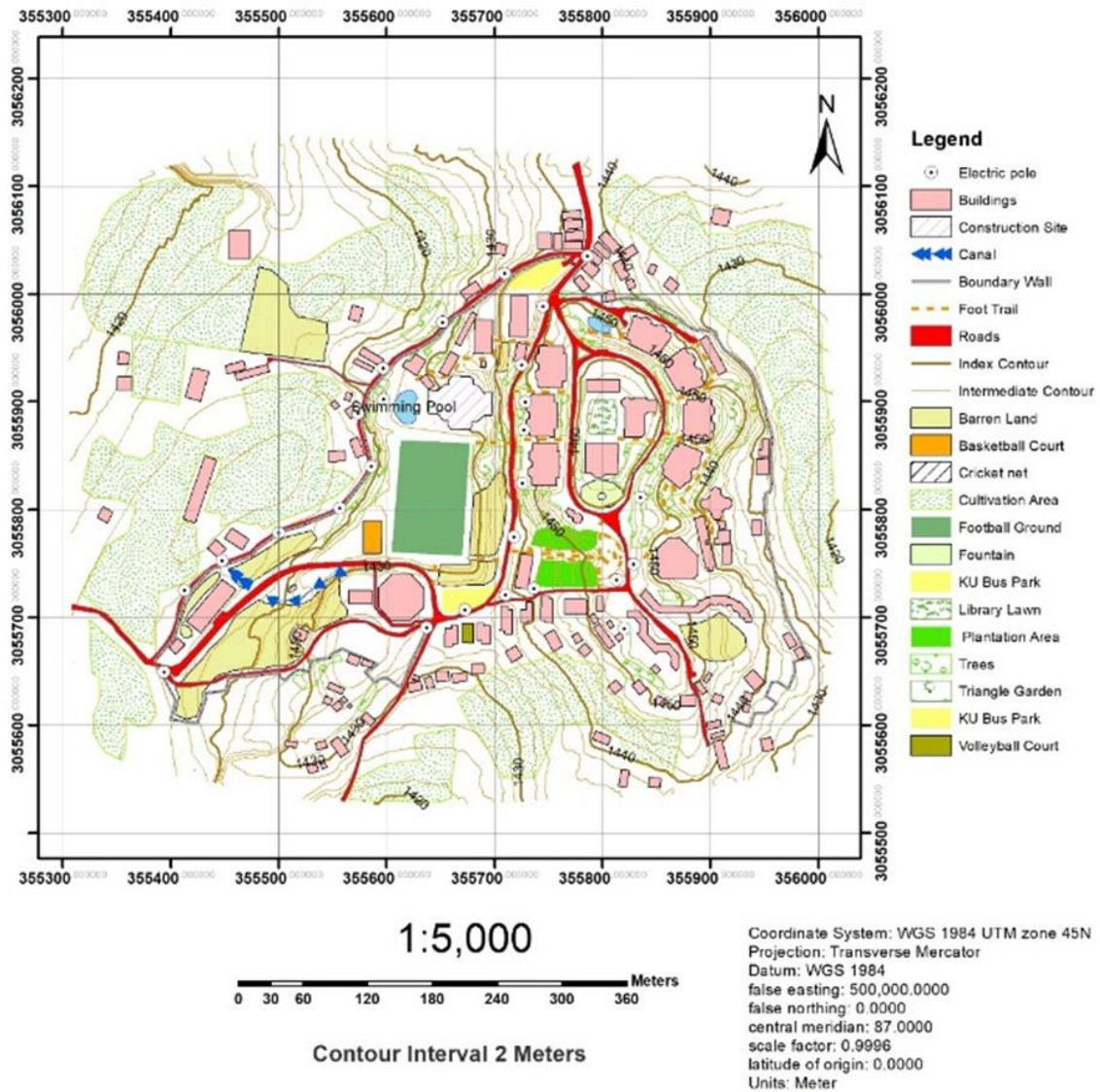


Figure 5. Topographic map of the study area

4.5. Topographic Map

Finally, the topographic map of the study area was prepared in GIS software (Figure 5). Land cover classification and utility mapping were also done. Similarly, contour lines were used in a 2m interval to show the shape of the Earth's surface. This map can be handy in carrying out any planning, designing, and construction activities on the given premises.

5. Conclusion and Recommendations

The primary aim of this project was to use UAVs for spatial data collection, create a high-resolution orthophoto, and later extract the features for mapping applications. Contour and topographic maps were made through photogrammetric and GIS processing, which have significant importance in various infrastructure and development planning. Similarly, the vector layer obtained after digitizing features, land use, and land covers can be helpful in land use planning, base, and cadastral map preparation, etc.

This study has ensured that UAV is a reliable and portable technology to acquire data remotely and provide a result with a very high spatial and temporal resolution even in inaccessible terrain at a relatively low cost. Furthermore, this study also unfolds the use of the HPC system for image processing which can be a game-changer in the future. For a developing country like Nepal, where Geospatial data is highly demanded, UAVs can be revolutionary for effective and rapid spatial data acquisition at low cost and time.

Furthermore, the HPC system and WebODM can be beneficial for decreasing the processing time. The HPC can be 10 to 20x faster than the PC at dense point cloud processing, depending on the number of HPC nodes and the total number of images [45]. It needs further research for improvement and a better conclusion. Similarly, the image orientation without GCPs is still less accurate for high-precision work. At the same time, the use of GCPs will consequently consume extra time for field and office work and give more accuracy.

Acknowledgement

We want to thank Kathmandu University, the Department of Geomatics Engineering, Dhruva Aryal, Sayam Baidar, and all other helping hands for the coordination during data acquisition and image processing.

This research was supported in part through computational resources provided by the Supercomputer Center Kathmandu University, which was established with equipments donated by CERN.

Author contributions

Abinash Silwal: Conceptualization, Methodology, Software, Data curation, Writing-Original, Editing. **Sunil Tamang:** Draft preparation, Software, Validation. **Rajendra Adhikari:** Visualization, Investigation, Reviewing, and Editing.

Conflicts of interest

The authors declare no conflicts of interest.

References

1. Stock, K., & Guesgen, H. (2016). Geospatial reasoning with open data. In *Automating open source intelligence* (pp. 171-204). Syngress.
2. <https://www.gim-international.com/content/blog/the-role-of-spatial-data-and-technologies-towards-building-smart-nations>
3. <https://documents.worldbank.org/en/publication/documents-reports/documentdetail/358501495199225866/climbing-higher-toward-a-middle-income-nepal>
4. <https://blogs.worldbank.org/sustainablecities/reversing-geospatial-digital-divide-one-step-or-leap-time>
5. Batty, M. (2016). Big data and the city. *Built Environment*, 42(3), 321-337.
6. Pérez, M., Agüera, F., & Carvajal, F. (2013). Low cost surveying using an unmanned aerial vehicle. *Int. Arch. Photogramm. Remote Sens. Spat. Inf. Sci*, 40, 311-315.
7. Green, D. R., Hagon, J. J., Gómez, C., & Gregory, B. J. (2019). Using low-cost UAVs for environmental monitoring, mapping, and modelling: Examples from the coastal zone. In *Coastal management* (pp. 465-501). Academic Press.
8. Shahbazi, M., Théau, J., & Ménard, P. (2014). Recent applications of unmanned aerial imagery in natural resource management. *GIScience & Remote Sensing*, 51(4), 339-365.
9. Colomina, I., & Molina, P. (2014). Unmanned aerial systems for photogrammetry and remote sensing: A review. *ISPRS Journal of photogrammetry and remote sensing*, 92, 79-97.
10. Aber, J. S., Marzolf, I., Ries, J. B., & Aber, S. E. (2019). Unmanned Aerial Systems. *Small-Format Aerial Photography and UAS Imagery*, 119-139.
11. Estrada, M. A. R., & Ndoma, A. (2019). The uses of unmanned aerial vehicles-UAV's-(or drones) in social logistic: Natural disasters response and humanitarian relief aid. *Procedia Computer Science*, 149, 375-383.
12. Ahmad, A., & Samad, A. M. (2010, May). Aerial mapping using high resolution digital camera and unmanned aerial vehicle for Geographical Information System. In *2010 6th International Colloquium on Signal Processing & its Applications* (pp. 1-6). IEEE.
13. Everaerts, J. (2008). The use of unmanned aerial vehicles (UAVs) for remote sensing and mapping. *The International Archives of the Photogrammetry, Remote Sensing and Spatial Information Sciences*, 37(2008), 1187-1192.
14. Choi, K., Lee, I., Hong, J., Oh, T., & Shin, S. W. (2009, April). Developing a UAV-based rapid mapping system for emergency response. In *Unmanned Systems Technology XI* (Vol. 7332, pp. 75-86). SPIE.
15. Zolkepli, M. F., Ishak, M. F., Yunus, M. Y. M., Zaini, M. S. I., Wahap, M. S., Yasin, A. M., ... & Hezmi, M. A. (2021). Application of unmanned aerial vehicle (UAV) for slope mapping at Pahang Matriculation College,

- Malaysia. *Physics and Chemistry of the Earth, Parts A/B/C*, 123, 103003.
16. Colomina, I., & Molina, P. (2014). Unmanned aerial systems for photogrammetry and remote sensing: A review. *ISPRS Journal of photogrammetry and remote sensing*, 92, 79-97.
 17. Ardi, N. D., Iryanti, M., Asmoro, C. P., Nurhayati, N., & Agustine, E. (2018, April). Mapping landslide potential area using fault fracture density analysis on unmanned aerial vehicle (UAV) image. In *IOP Conference Series: Earth and Environmental Science* (Vol. 145, No. 1, p. 012010). IOP Publishing.
 18. Nex, F., Armenakis, C., Cramer, M., Cucci, D. A., Gerke, M., Honkavaara, E., ... & Skaloud, J. (2022). UAV in the advent of the twenties: Where we stand and what is next. *ISPRS journal of photogrammetry and remote sensing*, 184, 215-242.
 19. Watts, A. C., Ambrosia, V. G., & Hinkley, E. A. (2012). Unmanned aircraft systems in remote sensing and scientific research: Classification and considerations of use. *Remote Sensing*, 4(6), 1671-1692.
 20. Chabot, D. (2018). Trends in drone research and applications as the Journal of Unmanned Vehicle Systems turns five. *Journal of Unmanned Vehicle Systems*, 6(1), vi-xv.
 21. Linchant, J., Lisein, J., Semeki, J., Lejeune, P., & Vermeulen, C. (2015). Are unmanned aircraft systems (UAS) the future of wildlife monitoring? A review of accomplishments and challenges. *Mammal Review*, 45(4), 239-252.
 22. Chabot, D., & Bird, D. M. (2015). Wildlife research and management methods in the 21st century: Where do unmanned aircraft fit in?. *Journal of Unmanned Vehicle Systems*, 3(4), 137-155.
 23. Laliberte, A. S., & Rango, A. (2011). Image processing and classification procedures for analysis of sub-decimeter imagery acquired with an unmanned aircraft over arid rangelands. *GIScience & Remote Sensing*, 48(1), 4-23.
 24. Wundram, D., & Löffler, J. (2008). High-resolution spatial analysis of mountain landscapes using a low-altitude remote sensing approach. *International Journal of Remote Sensing*, 29(4), 961-974.
 25. Immerzeel, W. W., Kraaijenbrink, P. D., Shea, J. M., Shrestha, A. B., Pellicciotti, F., Bierkens, M. F., & de Jong, S. M. (2014). High-resolution monitoring of Himalayan glacier dynamics using unmanned aerial vehicles. *Remote Sensing of Environment*, 150, 93-103.
 26. Lucieer, A., Jong, S. M. D., & Turner, D. (2014). Mapping landslide displacements using Structure from Motion (SfM) and image correlation of multi-temporal UAV photography. *Progress in physical geography*, 38(1), 97-116.
 27. Zhang, C., & Kovacs, J. M. (2012). The application of small unmanned aerial systems for precision agriculture: a review. *Precision agriculture*, 13(6), 693-712.
 28. Samseemoung, G., Soni, P., Jayasuriya, H. P., & Salokhe, V. M. (2012). Application of low altitude remote sensing (LARS) platform for monitoring crop growth and weed infestation in a soybean plantation. *Precision Agriculture*, 13(6), 611-627.
 29. Herwitz, S. R., Johnson, L. F., Dunagan, S. E., Higgins, R. G., Sullivan, D. V., Zheng, J., ... & Brass, J. A. (2004). Imaging from an unmanned aerial vehicle: agricultural surveillance and decision support. *Computers and electronics in agriculture*, 44(1), 49-61.
 30. Mancini, F., Dubbini, M., Gattelli, M., Stecchi, F., Fabbri, S., & Gabbianelli, G. (2013). Using unmanned aerial vehicles (UAV) for high-resolution reconstruction of topography: The structure from motion approach on coastal environments. *Remote sensing*, 5(12), 6880-6898.
 31. Bemis, S. P., Micklethwaite, S., Turner, D., James, M. R., Akciz, S., Thiele, S. T., & Bangash, H. A. (2014). Ground-based and UAV-Based photogrammetry: A multi-scale, high-resolution mapping tool for structural geology and paleoseismology. *Journal of Structural Geology*, 69, 163-178.
 32. Jensen, A. M., Morgan, D., Chen, Y., Clemens, S., & Hardy, T. (2009, January). Using multiple open-source low-cost unmanned aerial vehicles (UAV) for 3D photogrammetry and distributed wind measurement. In *International Design Engineering Technical Conferences and Computers and Information in Engineering Conference* (Vol. 49002, pp. 629-634).
 33. Boon, M. A., Greenfield, R., & Tesfamichael, S. (2016). Unmanned aerial vehicle (UAV) photogrammetry produces accurate high-resolution orthophotos, point clouds and surface models for mapping wetlands. *South African Journal of Geomatics*, 5(2), 186-200.
 34. Chi, Y. Y., Lee, Y. F., & Tsai, S. E. (2016, October). Study on high accuracy topographic mapping via uav-based images. In *IOP Conference Series: Earth and Environmental Science* (Vol. 44, No. 3, p. 032006). IOP Publishing.
 35. Quaye-Ballard, N. L., Asenso-Gyambibi, D., & Quaye-Ballard, J. (2020). Unmanned Aerial Vehicle for Topographical Mapping of Inaccessible Land Areas in Ghana: A Cost-Effective Approach.
 36. Azmi, S. M., Ahmad, B., & Ahmad, A. (2014, February). Accuracy assessment of topographic mapping using UAV image integrated with satellite images. In *IOP Conference Series: Earth and Environmental Science* (Vol. 18, No. 1, p. 012015). IOP Publishing.
 37. Raid, A. T., Arthur, M., & Davis, D. (2011). Low-cost aerial mapping alternatives for natural disasters in the Caribbean. FIG Working Week.
 38. Eisenbeiss, H., & Sauerbier, M. (2011). Investigation of UAV systems and flight modes for photogrammetric applications. *The Photogrammetric Record*, 26(136), 400-421.
 39. Su, L., Huang, Y., Gibeau, J., & Li, L. (2016). The index array approach and the dual tiled similarity algorithm for UAS hyper-spatial image processing. *GeoInformatica*, 20(4), 859-878.
 40. Singh, K. K., & Frazier, A. E. (2018). A meta-analysis and review of unmanned aircraft system (UAS) imagery for terrestrial applications. *International Journal of Remote Sensing*, 39(15-16), 5078-5098.
 41. <https://www.opendronemap.org/webodm/>
 42. Nex, F., & Remondino, F. (2014). UAV for 3D mapping applications: a review. *Applied geomatics*, 6(1), 1-15.

43. Ahmad, M. J., Ahmad, A., & Kanniah, K. D. (2018, June). Large scale topographic mapping based on unmanned aerial vehicle and aerial photogrammetric technique. In *IOP Conference Series: Earth and Environmental Science* (Vol. 169, No. 1, p. 012077). IOP Publishing.
44. Udin, W. S., & Ahmad, A. (2014, February). Assessment of photogrammetric mapping accuracy based on variation flying altitude using unmanned aerial vehicle. In *IOP conference series: earth and environmental science* (Vol. 18, No. 1, p. 012027). IOP Publishing.
45. Gillan, J. K., Ponce-Campos, G. E., Swetnam, T. L., Gorlier, A., Heilman, P., & McClaran, M. P. (2021). Innovations to expand drone data collection and analysis for rangeland monitoring. *Ecosphere*, 12(7), e03649.



© Author(s) 2022. This work is distributed under <https://creativecommons.org/licenses/by-sa/4.0/>



Mersin Photogrammetry Journal

<https://dergipark.org.tr/en/pub/mephoj>

e-ISSN 2687-654X



Detection and documentation of stone material deterioration in historical masonry buildings using UAV photogrammetry: A case study of Mersin Sarışih Inn

Lale Karataş¹, Aydın Alptekin², Atilla Karabacak³, Murat Yakar⁴

¹Mardin Artuklu University, Department of Architecture and Urban Planning, Mardin, Türkiye

²Mersin University, Department of Geological Engineering, Mersin, Türkiye

³Mersin University, Vocational School of Technical Sciences, Department of Architecture and Urban Planning, Mersin, Türkiye

⁴Mersin University, Geomatics Engineering Department, Mersin, Türkiye

Keywords

Remote sensing
UAV
Photogrammetry
DEM
Camera Calibration

Research Article

DOI:10.53093/mephoj.1198605

Received: 02.11.2022

Revised: 05.12.2022

Accepted: 19.12.2022

Published: 22.12.2022

Abstract

Detection of material degradation of urban facades constitutes a preliminary activity for the preparation of any restoration response project. The traditional method for fixation relies on mechanical contact means and requires a great time effort to obtain a few preliminary points. In addition, the size of buildings and historical places make it difficult to examine the types of material deterioration, and on-site visual analyzes and current inspections by experts can also lead to human-induced errors. The development of methods based on UAV photogrammetry in order to reduce the labor force and margin of error in solving this situation brings great convenience for the detection of material deterioration in historical areas. The aim of the study carried out in this context is to document the material problems of "Sarışih Han", a historical masonry building located in the Tarsus district of Mersin, which is of great importance for its continuity. Contributing to the documentation, detection and repair of financial problems for the preservation of the cultural heritage of the region and thus the sustainable management of the structures in the geographical region. In this context, material problems in the structure were documented using UAV photogrammetry method. In the study, the use of UAV photogrammetry to support the constraints of material deteriorations allows for more detailed results in façade analysis of material deteriorations, leading to simplification of manual and direct search procedures.

1. Introduction

Historical buildings are heritage sites that ensure the sustainability of collective memories such as the lifestyles and beliefs of past societies. Stone, which is the most used material in movable and immovable cultural heritage in these areas, which helps to reconstruct history, is under threat due to deterioration processes due to various reasons. These deteriorations in historical buildings are caused by natural environmental factors such as meteorological conditions and anthropological factors such as air pollution, as well as the properties of the materials that make up the building. For example, rain water, which is a natural factor, accelerates the dissolution processes after freezing / thawing cycles, and also increases the amount of deterioration by

accelerating the mechanical events in the structure of the stone by creating changes in the chemical structure of the stone [1]. In addition, the side exposed to water shows significant erosion in the limestones [2-10]. In addition, various studies in the literature report that the effect of water on stone structures tends to increase the acidity of atmospheric pollutants over time, which further increases erosion and color change in stones [11,12]. Failure to take control and precautions in stone deterioration caused by the effects of water can turn small-scale (for example, flaking, fragmentation, cracking) deterioration into larger-scale deterioration over time, and this may lead to loss of cultural traces in historical areas [13]. For this reason, pre-detection and mapping of material deterioration in order to take the

* Corresponding Author

(karataslale@gmail.com) ORCID ID 0000-0001-8582-4612
(aydinalptekin@mersin.edu.tr) ORCID ID 0000-0002-5605-0758
(atilakarabacak@mersin.edu.tr) ORCID ID 0000 - 0002 - 1096 - 3949
(myakar@mersin.edu.tr) ORCID ID 0000-0002-2664-625

Cite this article

Karataş, L. Alptekin, A., Karabacak, A., & Yakar, M. (2022). Detection and documentation of stone material deterioration in historical masonry buildings using UAV photogrammetry: A case study of Mersin Sarışih Inn. *Mersin Photogrammetry Journal*, 4(2), 53-61

necessary measures is one of the most important stages of restoration works in the protection of heritage in historical areas.

Material degradation mapping of urban facades constitutes a preliminary activity for preparing any restoration response project. The traditional method for mapping relies on mechanical contact means and requires a great deal of time effort to obtain several front points [1]. In addition, the size of the building and historical sites makes it difficult to examine the types of material deterioration, and on-site visual analysis and up-to-date inspections by experts can also lead to human-induced errors. The development of methods based on various technologies in order to reduce the labor force and margin of error in the solution of this situation brings great convenience for the detection of material deterioration in historical areas [13]. In addition, the use of digital tools to support mapping activities allows for more detailed results on façade analysis [14] leading to simplification of manual and direct survey procedures [1].

In the literature, it is defined that the method that represents the best solution for the detection of material deterioration on facades should be tools that can obtain both spatial (XYZ) and RGB data by allowing the combination of geometric and material information. In the literature, in the detection of stone material deterioration, devices such as terrestrial laser scanning and photogrammetry are supported by computer software, and studies on surface erosion investigation and pixel-based material properties determination confirm the usability of these methods for material properties. However, although all these methods have important advantages in heritage areas, it has been determined by various studies that they have some inadequacies in the detection of material deterioration. For example, although Terrestrial Laser Scanning (TLS)-based surveys used to detect material deterioration allow us to obtain dense point clouds, obtain sufficient geometric data to be used in the modeling process for facades [15], due to the low resolution in RGB data, they are insufficient for distortion mapping [16]. The most important of these inadequacies in the terrestrial laser scanning method is the fact that the distortion groups are different from each other in shape, texture and color, and the distortion groups must have sufficient resolution for the interpretation of the data during identification. Other disadvantages are that they are expensive and data processing times are long. In some TLS devices, this is partially resolved by adding an external high-performance digital camera or by adding a digital camera. Digital close-range photogrammetry, on the other hand, is still subject to limitations in material deterioration, as it is time consuming and requires high labor force to record every area of the structures due to the location of the camera angle [17]. In addition, techniques such as terrestrial laser scanning and photogrammetry are insufficient to easily visualize the area, especially in historical urban contexts with narrow streets and tall buildings. A close-range photogrammetric survey study to analyze the material deterioration of a large historic building facade in Bologna (Italy) shows that this technique can only be

used in structures that can be closely examined and detected in situ, and that the size of the areas makes it difficult to study the types of deterioration and the use of different technologies to compensate for these disadvantages. reported that it would be useful in the detection of material deterioration.

Various studies in the literature emphasize the importance of using UAVs in the detection of material deterioration as a method to overcome the disadvantages of methods such as terrestrial laser scanning and photogrammetry. Russo et al. [1] studied material deterioration detection by drone technology, and found that this technique is an efficient method to support restoration analysis because it is low cost, fast and easy to use in material deterioration mapping. It has also been confirmed by various studies that UAV technology is a good method to overcome terrain limitations and to search for hidden front areas [18-20].

Remote sensing technologies have been frequently used in engineering projects in the last decade [21-36]. In this context, it is aimed to identify and document the material problems of the "Sarıışık Han" building, which is located in the Tarsus district of Mersin, which is the subject of the study, and which is of great importance to be preserved in terms of the continuity of the cultural heritage of the region, by using UAV photogrammetry, which is emphasized to be of great convenience in detecting material problems in the literature. Thus, it will contribute to the detection and repair of material problems for the sustainable management of buildings in the geographical region. In this context, within the scope of the study, firstly, information about the historical importance and spatial situation of the "Sarıışık Han" building was given, and in the next step, how the building was documented using UAV photogrammetry was explained in the method section. In the results section, the stone material problems in the building, which were determined by using the data obtained from UAV photogrammetry, are included, and in the conclusion section, intervention suggestions for the repair of the detected material problems are presented.

2. Study Area

Tarsus has been an important administrative, commercial and military center since ancient times due to its strategic location. Connecting Central Anatolia to Çukurova and Northern Syria the caravanserai, located on the right arm of Anatolia and on the route where the Pilgrimage route passes, is on the Tarsus-Pozantı Road near Gülek Pass and 90 km from Tarsus. The caravanserai, which is within the borders of Çukurbağ Village of Tarsus district of Mersin, is located in Sarı Işık (Sarıışık) Neighborhood. Caravanserai is called "Sarı Işık Han" or "Sarıışık Han" by the villagers (Figure 1).

The building was built on a land that slopes from south to north. On the eastern façade, it is seen that most of the outer cladding has been shed. Again, on this façade, there are three shapeless openings made later in the wall. The building was used for soda production for a period, and during this use, large openings were probably created on the eastern wall. The top of the building is completely covered with concrete, laterally inclined in

two directions. The northeastern corner of the building, which is in a very neglected condition today, is about to be demolished. It is noteworthy that the exterior coating on the north and west façades has been renewed from place to place. This repair was made in the 1970s. There are crenellated windows in the upper part of the north and south façades. The caravanserai, which has a rectangular plan and a single closed space extending in the north-south direction, was built with coarse stones

and rubble. The low-arched entrance, located on the western façade from the long sides, is arranged in the form of an iwan protruding from the façade. The entrance iwan is covered with a pointed arched vault. The side walls and vault of the entrance iwan are partially collapsed. The top of the single-room caravanserai is covered with a north-south oriented pointed arched vault parallel to the entrance façade. The vault is connected by eight support arches.

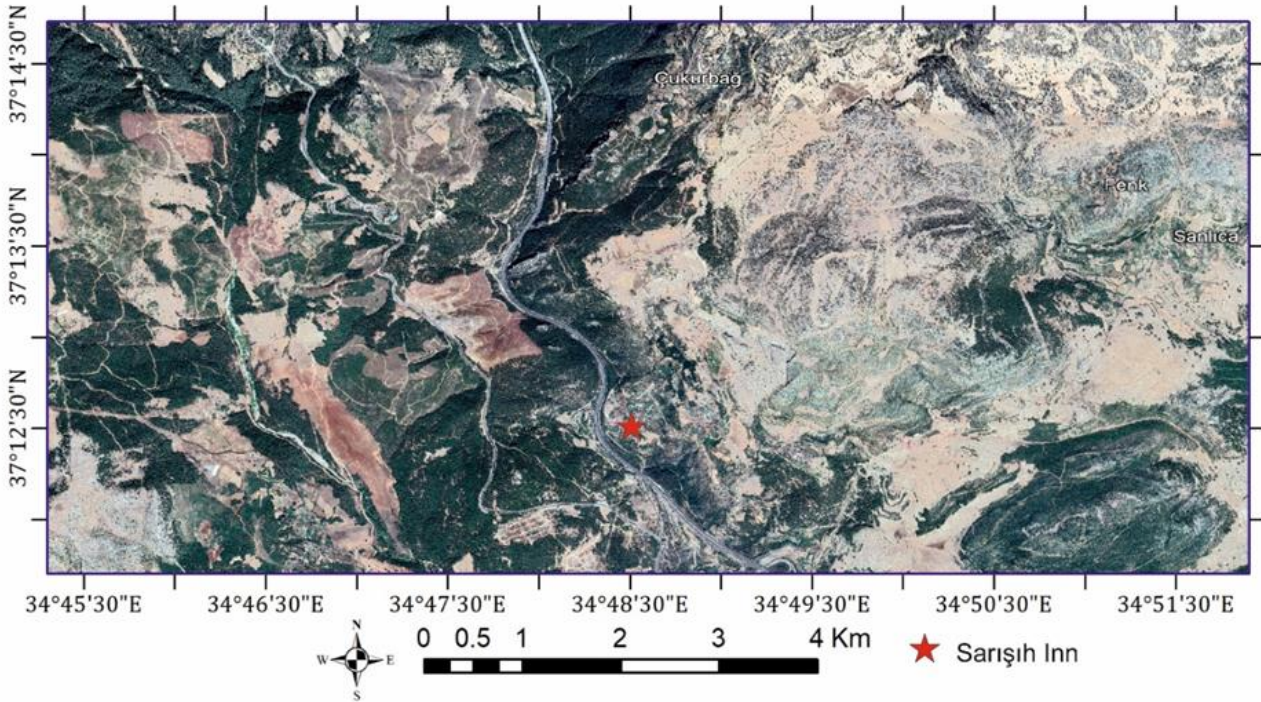


Figure 1. Location map

3. Method

This study consists of two stages: field and office work. Controlling the study area, preparing it to be photographed, and taking images of the caravanserai with an unmanned aerial vehicle constitute the field study phase. During the office work phase, the data taken from the unmanned aerial vehicle was transferred to the computer environment, interpreted and processed. The images collected in the field by the UAV photogrammetry method were transferred to the computer in the office environment and the classification of the types of deterioration in the building was made. The deterioration of the stone material in the building has been mapped by considering the International Stone Scientific Committee (ICOMOS-ISCS) classification prepared according to the International Council of Monuments [37,38]. Identified material deteriorations are tabulated by dividing them into classes on the basis of stone building elements in masonry structures.

In the literature, the structural elements seen in masonry structures are defined as vertical carriers, horizontal carriers, stairs, wall cavities and auxiliary elements [39,40]. Vertical carriers in the building are defined as pillars, columns and walls. There is no use of pillars or columns in the building. Horizontal carriers from the building elements are defined as floors. Flat flooring is used in the building. In the literature, auxiliary

elements in stone structures are defined as gargoyles, ornaments, moldings, and no auxiliary elements were used in the structure.

3.1. Field study

At this stage of the study, first of all, the necessary permissions were obtained to fly in the Tarsus District of Mersin Province, which is the study area. Images were captured manually with a Parrot Anafi HDR drone (Figure 2). The technical properties of drone are shown in Table 1. Every detail of the structure was tried to be captured by flying first at low altitude and then at high altitude. During the photo shoots, the camera was calibrated beforehand and 101 photos were taken without any changes in the parameters. A smartphone was used together with the remote control during the photo shoot. Free Flight 6 and Pix4D Capture applications have been installed in order for the smartphone and the remote to work integrated.

3.2. Office work

After the completion of the image acquisition within the scope of the field work, the office work phase was started. First of all, the data obtained from the field were transferred to the computer environment. The pictures taken were examined in detail and material deteriorations were detected. From the images collected

in the field by the UAV photogrammetry method, the pictorial dictionary published by ICOMOS and the findings regarding the material deteriorations summarized in Table 2.



Figure 2. Anafi Parrot

Table 1. Technical specifications of the UAV (Parrot 2021)

Feature	Value
Drone	
Size folded	244x67x65 mm
Size unfolded	175x240x65 mm
Weight	320 g
Max transmission range	4km with controller
Max flight time	25 min
Max horizontal speed	15 m/s
Max vertical speed	4 m/s
Max wind resistance	50 km/h
Service ceiling	4500m above sea level
Operating temperature	-10°C to 40°C
Lens	
Sensor	1/2.4" CMOS
Aperture	f/2.4
Focal length (35 mm eq.)	23-69 mm (photo)
Depth of field	1.5 m - ∞
ISO range	100-3200
Digital zoom	up to 3x (4K Cinema, 4K UHD, FHD)
Photo resolution	21MP (5344x4016) / 4:3 / 84° HFOV

Table 2. Stone material deterioration in the structural elements of the building

NATURAL STONE CONSTRUCTION ELEMENTS			PROBLEMS ENCOUNTERED ON CONSTRUCTION ELEMENTS MADE OF MASONRY MATERIAL																				
			Loss of surface	Fragmentation	Formation of gap/ hole	Pitting	Cracks	Spalling	Foliation	Discharge of jointing	Surface contamination	Shell formation	Efflorescence	Crystallization	Formation of plant	Formation of moss	Corrosion (Rust stain)	Tear	Loss of form	Colour change	Faulty Repairs		
VERTICAL BEARINGS	SINGLE BEARINGS	Leg	-	-	-	-	-	-	-	-	-	-	-	-	-	-	-	-	-	-	-	-	-
		Column	-	-	-	-	-	-	-	-	-	-	-	-	-	-	-	-	-	-	-	-	-
VERTICAL BEARINGS	CONTINUOUS BEARINGS	Wall	-	-	-	-	-	-	x	x	-	-	-	x	-	-	-	-	x	-	-	-	
		Flat	-	-	-	-	-	-	-	-	-	-	-	-	-	-	-	-	-	-	-	-	-
HORIZONTAL BEARINGS	FLOORINGS	Curvilinear	-	-	-	-	-	-	-	-	-	-	-	-	-	-	-	-	-	-	-	-	
		Window	Lintel / jamb	-	-	-	-	-	-	-	-	-	-	-	-	-	-	-	-	-	-	-	-
WALL OPENINGS	Door	Sill	-	-	-	-	-	-	-	-	-	-	-	-	-	-	-	-	-	-	-	-	
		Lintel / jamb	-	-	-	-	-	-	-	-	-	-	-	-	-	-	-	-	-	-	-	-	-
		Sill	-	-	-	-	-	-	-	-	-	-	-	-	-	-	-	-	-	-	-	-	-
	Arch	-	-	-	-	-	-	-	-	-	-	-	-	-	-	-	-	-	-	-	-	-	-
AUXILIARY ELEMENTS	Network	-	-	-	-	-	-	-	-	-	-	-	-	-	-	-	-	-	-	-	-	-	
	Moulding	-	-	-	-	-	-	-	-	-	-	-	-	-	-	-	-	-	-	-	-	-	
	Gargoyle	-	-	-	-	-	-	-	-	-	-	-	-	-	-	-	-	-	-	-	-	-	
	Chimney	-	-	-	-	-	-	-	-	-	-	-	-	-	-	-	-	-	-	-	-	-	
	Element for passage to the cover	-	-	-	-	-	-	-	-	-	-	-	-	-	-	-	-	-	-	-	-	-	

4. Results

4.1. Deterioration in vertical carriers

In the literature, vertical carriers of building elements in masonry structures are defined as feet, columns and walls. There is no use of pillars or columns in the building. The deterioration in the walls of the building was determined as plant formation and joint loss. On the south façade of the building, there are plants growing in the areas close to the ground where joint loss and joint losses occur due to the effect of water. Joint discharge and plant formation problems were detected on the south façade of the building (Figure 3).

On the eastern façade of the building, vegetation, surface pollution, discoloration and joint discharge problems were detected (Figure 4).

Partial fragmentation problems were encountered as a result of the effects of the loads on the building

caused by the excess plant growth on the northern façade of the building (Figure 5).

4.2. Deterioration in horizontal carriers

In the literature, horizontal carriers from building elements in masonry structures are defined as floors. Flat flooring and vaulted roof use are seen in the entrance with iwan on the south façade. Vegetation type stone degradation is observed on the flat floor and the vaulted roof (Figure 6 and Figure 7).

4.3. Deterioration in auxiliary elements

In the literature, auxiliary elements of building elements in masonry structures are defined as gargoyles, ornaments and moldings. No auxiliary elements were found in the building.



(a) Plant formation



(b) Joint discharge

Figure 3. Stone material deteriorations detected on the south façade



(a) Plant formation



(b) Surface contamination



(c) Color change



(d) Joint discharge

Figure 4. Stone material deteriorations detected on the east façade



Figure 5. Fragment rupture

5. Discussion

The main purpose of the study is to identify and document the deterioration patterns of the stones that make up the structure of the "Sarışlı Han" located in the Tarsus district of Mersin. In order to investigate the deterioration patterns in the structure, the images obtained by UAV photogrammetry were interpreted considering the ICOMOS stone material classification and the types of deterioration were determined. In this context, the use of UAV photogrammetry to support stone material deterioration detection activities appears to lead to simplification of manual and direct detection procedures by providing more detailed results in the detection of material deterioration, façade analysis. As a result of the study, it has been seen that it is possible to detect material problem types down to the smallest detail based on visual inspection only, without an on-site observational examination, thanks to UAV photogrammetry. In addition, it is seen that UAV photogrammetry is an effective method to support restoration analysis because it saves manpower, labor and time in the detection of stone material problems, and this technique is low cost, fast and easy to detect material deterioration.

In addition, the results of the study show that this method is a useful method to compensate for the disadvantages of terrestrial laser scanning and conventional photogrammetry in detecting material deteriorations due to its low cost and low data processing time [15,16]. In the study process, material deteriorations were easily detected on the images obtained from UAV photogrammetry without the need for on-site inspection of the structure. This finding supports the results of studies that found UAV technology to be a good method to circumvent terrain limitations and search for concealed front areas [18-20].

Another important finding obtained from the study is that the material problems detected in the data

obtained by the UAV method are plant formation, joint discharge, surface pollution and color change. It is seen that the problem of plant formation and joint grooves is dominant in a large part of the building. While the water entering the body wall eroded the joints, causing joint discharge, the water effect between the drained joints created the necessary environment for various living things to live in the province. This finding supports that the side exposed to water in limestones, which was also determined in the results of various studies in the literature, shows significant wear and therefore there are problems related to the abrasive effect of water on all facades exposed to water [2-10].

In addition, in the determinations made in the study, it is seen that the deterioration patterns in plant formation generally cause plant formation in the joint spaces thanks to the environment provided by rain water. This finding confirms that if control and precautions are not taken against rain water, which is a natural factor mentioned in various studies, small-scale deterioration (such as flaking, flaking, etc.), fragmentation, cracking can turn into larger-scale deteriorations such as plant formation over time [1,13].

Another important finding obtained in the study, the gray layer called surface pollution, draws attention on the facades except the south façade, where the residence time of water on the wall is longer. This situation suggests the fact that the water evaporates faster from the wall of the building due to the sunshine duration on the south façade and causes a color change in this situation, while on the north façade, the water stays in contact with the body wall more and evaporates slowly, so it can clean the black layer caused by the pollution on the façade less. This finding supports the fact that the acidity of the water tends to increase over time due to the atmospheric pollutants obtained in the results of Fort et al [11] and Castaño González et al. [12], which further increases the erosion and color change in the stones.

6. Conclusion

In the study presented in this article, UAV photogrammetry was used to investigate the deterioration patterns of the building material of the "Sarışih Hanı" building, which is one of the most important buildings in terms of the sustainability of the cultural heritage in Mersin, and the deterioration types were determined by interpreting the images obtained. In this context, the use of UAV photogrammetry to support stone material deterioration detection activities appears to lead to simplification of manual and direct detection procedures by providing more detailed results in the detection of material deterioration, façade analysis.

The results show that the main damage observed on the stone surface of the building is the erosion by the effect of water and the problems caused by the lack of repairs in the worn areas, and plant formations occur in almost all parts of the facades and the plant formations cause large fragmentation on some facades. It is seen that the joint loss on the stone surfaces and the deterioration of plant formation have reached advanced levels as a result of the exposure of the building to the effects of sun and water caused by the strong climate for centuries. Restoration methods should be tried to stabilize the deterioration and replace the most degraded stones. To treat surface contamination degradation, consideration should be given to removing the gray layer to increase the stone's resilience to environmental pollution and to prevent subsequent exposure to weathering.

Author contributions

Lale Karataş: Conceptualization, Methodology, Software
Aydın Alptekin: Data curation, Writing-Original draft preparation, Software, Validation. **Atilla Karabacak:** Field study, Editing **Murat Yakar:** Visualization, Investigation, Writing-Reviewing and Editing.

Conflicts of interest

The authors declare no conflicts of interest.

References

- Russo, M., Carnevali, L., Russo, V., Savastano, D., & Taddia, Y. (2019). Modeling and deterioration mapping of façades in historical urban context by close-range ultra-lightweight UAVs photogrammetry. *International journal of architectural heritage*, 13(4), 549-568.
- Bonazza, A., Vidorni, G., Natali, I., Ciantelli, C., Giosuè, C., & Tittarelli, F. (2017). Durability assessment to environmental impact of nano-structured consolidants on Carrara marble by field exposure tests. *Science of the Total Environment*, 575, 23-32.
- Gulotta, D., Bontempi, E., Bugini, R., Goidanich, S., & Toniolo, L. (2017). The deterioration of metamorphic serpentinites used in historical architecture under atmospheric conditions. *Quarterly Journal of Engineering Geology and Hydrogeology*, 50(4), 402-411.
- Waragai, T., & Hiki, Y. (2019). Influence of microclimate on the directional dependence of sandstone pillar weathering in Angkor Wat temple, Cambodia. *Progress in Earth and Planetary Science*, 6(1), 1-14.
- Bello, M. A., Martin, L., & Martin, A. (1992). Decay and treatment of macael white marble. *Studies in conservation*, 37(3), 193-200.
- Sarró, M. I., García, A. M., Rivalta, V. M., Moreno, D. A., & Arroyo, I. (2006). Biodeterioration of the lions fountain at the Alhambra Palace, Granada (Spain). *Building and Environment*, 41(12), 1811-1820.
- Sanjurjo-Sánchez, J., & Alves, C. (2012). Decay effects of pollutants on stony materials in the built environment. *Environmental Chemistry Letters*, 10(2), 131-143.
- Germinario, L., Siegesmund, S., Maritan, L., Simon, K., & Mazzoli, C. (2017). Trachyte weathering in the urban built environment related to air quality. *Heritage Science*, 5(1), 1-17.
- Germinario, L., Oguchi, C. T., Tamura, Y., Ahn, S., & Ogawa, M. (2020). Taya Caves, a Buddhist marvel hidden in underground Japan: stone properties, deterioration, and environmental setting. *Heritage Science*, 8(1), 1-20.
- Winkler, E. (1997). *Stone in architecture: properties, durability*. Springer Science & Business Media.
- González, R. F., De Buergo, M. A., Martín, F. M., & De Azcona, M. L. (2004). Stone decay in 18th century monuments due to iron corrosion. The Royal Palace, Madrid (Spain). *Building and Environment*, 39(3), 357-364.
- Castaño González, J. G., López de Azcona, C., & Morcillo Linares, M. (2001). Deterioration of ancient metallic elements taken from Toledo cathedral. *Revista De Metalurgia*, 37(4), 519-527
- Hatır, E., Korkanç, M., Schachner, A., & İnce, İ. (2021). The deep learning method applied to the detection and mapping of stone deterioration in open-air sanctuaries of the Hittite period in Anatolia. *Journal of Cultural Heritage*, 51, 37-49.
- Del Pozo, S., Herrero-Pascual, J., Felipe-García, B., Hernández-López, D., Rodríguez-González, P., & González-Aguilera, D. (2016). Multispectral radiometric analysis of façades to detect pathologies from active and passive remote sensing. *Remote Sensing*, 8(1), 80.
- Guidi, G., Russo, M., & Angheluddu, D. (2014). 3D survey and virtual reconstruction of archeological sites. *Digital Applications in Archaeology and Cultural Heritage*, 1(2), 55-69.
- Soudarissanane, S., Lindenbergh, R., Menenti, M., & Teunissen, P. (2011). Scanning geometry: Influencing factor on the quality of terrestrial laser scanning points. *ISPRS journal of photogrammetry and remote sensing*, 66(4), 389-399.
- Kraus, K. (2007). *Photogrammetry: geometry from images and laser scans* (Vol. 1). Walter de Gruyter.

18. Remondino, F., Spera, M. G., Nocerino, E., Menna, F., & Nex, F. (2014). State of the art in high density image matching. *The photogrammetric record*, 29(146), 144-166.
19. Fernández-Hernandez, J., González-Aguilera, D., Rodríguez-Gonzálvez, P., & Mancera-Taboada, J. (2015). Image-based modelling from unmanned aerial vehicle (UAV) photogrammetry: an effective, low-cost tool for archaeological applications. *Archaeometry*, 57(1), 128-145.
20. Hatır, E., Korkanç, M., Schachner, A., & İnce, İ. (2021). The deep learning method applied to the detection and mapping of stone deterioration in open-air sanctuaries of the Hittite period in Anatolia. *Journal of Cultural Heritage*, 51, 37-49.
21. Doğan, Y., & Yakar, M. (2018). GIS and three-dimensional modeling for cultural heritages. *International Journal of Engineering and Geosciences*, 3(2), 50-55.
22. Yakar, M. (2009). Digital elevation model generation by robotic total station instrument. *Experimental Techniques*, 33(2), 52-59.
23. Alptekin, A., Çelik, M. Ö., & Yakar, M. (2019). Anıtmezarın yersel lazer tarayıcı kullanarak 3B modellenmesi. *Türkiye Lidar Dergisi*, 1(1), 1-4.
24. Yılmaz, H. M., Yakar, M., Mutluoğlu, O., Kavurmacı, M. M., & Yurt, K. (2012). Monitoring of soil erosion in Cappadocia region (Selime-Aksaray-Turkey). *Environmental Earth Sciences*, 66(1), 75-81.
25. Yakar, M., Yılmaz, H. M., & Mutluoğlu, Ö. (2010). Close range photogrammetry and robotic total station in volume calculation. *International Journal of Physical Sciences*, 5(2), 86-96
26. Alptekin, A., & Yakar, M. (2020). Heyelan bölgesinin İHA kullanarak modellenmesi. *Türkiye İnsansız Hava Araçları Dergisi*, 2(1), 17-21.
27. Taşdemir, Ş., Yakar, M., Ürkmez, A., & İnal, Ş. (2008, June). Determination of body measurements of a cow by image analysis. In *Proceedings of the 9th International Conference on Computer Systems and Technologies and Workshop for PhD Students in Computing* (pp. V-8).
28. Unal, M., Yakar, M., & Yildiz, F. (2004, July). Discontinuity surface roughness measurement techniques and the evaluation of digital photogrammetric method. In *Proceedings of the 20th international congress for photogrammetry and remote sensing, ISPRS* (Vol. 1103, p. 1108).
29. Erener, A., & Yakar, M. (2012). Monitoring coastline change using remote sensing and GIS technologies. *Lecture Notes in Information Technology*, 30, 310-314.
30. Karataş, L., Alptekin, A., & Yakar, M. (2022). Creating Architectural Surveys of Traditional Buildings with the Help of Terrestrial Laser Scanning Method (TLS) and Orthophotos: Historical Diyarbakır Sur Mansion. *Advanced LiDAR*, 2(2), 54-63.
31. Karataş, L., Alptekin, A., & Yakar, M. (2022). Determination of Stone Material Deteriorations on the Facades with the Combination of Terrestrial Laser Scanning and Photogrammetric Methods: Case Study of Historical Burdur Station Premises. *Advanced Geomatics*, 2(2), 65-72.
32. Karataş, L., Alptekin, A., & Yakar, M. (2022). Analytical Documentation of Stone Material Deteriorations on Facades with Terrestrial Laser Scanning and Photogrammetric Methods: Case Study of Şanlıurfa Kışla Mosque. *Advanced LiDAR*, 2(2), 36-47.
33. Karataş, L., Alptekin, A., & Yakar, M. (2022). Material deteriorations occurring on the facades of the Mor Sergios Bakhos Church. *Advanced Engineering Days (AED)*, 4, 48-51.
34. Karataş, L., Alptekin, A., Kanun, E., & Yakar, M. (2022). Tarihi kârgir yapılarda taş malzeme bozulmalarının İHA fotogrametrisi kullanarak tespiti ve belgelenmesi: Mersin Kanlıdivane ören yeri vaka çalışması. *İçel Dergisi*, 2(2), 41-49.
35. Kanun, E., Alptekin, A., Karataş, L., & Yakar, M. (2022). The use of UAV photogrammetry in modeling ancient structures: A case study of “Kanytellis”. *Advanced UAV*, 2(2), 41-50.
36. Karataş, L., Alptekin, A., & Yakar, M. (2022). Detection and documentation of stone material deterioration in historical masonry structures using UAV photogrammetry: A case study of Mersin Aba Mausoleum. *Advanced UAV*, 2(2), 51-64.
37. Fitzner, B., Heinrichs, K., & La Bouchardiere, D. (2003). Weathering damage on Pharaonic sandstone monuments in Luxor-Egypt. *Building and Environment*, 38(9-10), 1089-1103.
38. ICOMOS-ISCS (2008). Illustrated Glossary on Stone Deterioration Patterns, Champigny/Marne, France.
39. Karataş, L. (2016). Mardin Kentsel Sit Alanındaki İbadet Yapılarında Malzeme Kullanımı ve Sorunları Üzerine Bir Araştırma. Master's Thesis, Uludağ University, Fen Bilimleri Enstitüsü, Bursa, 340p.
40. Karataş, L., Alptekin, A., & Yakar, M. (2022). Investigation of Molla Hari (Halil) Süleyman Paşa Mosque's material deteriorations. *Advanced Engineering Days (AED)*, 4, 55-57.





Application of terrestrial photogrammetry method in cultural heritage studies: A case study of Seyfeddin Karasungur

Adem Kabadayı*¹, Alperen Erdoğan¹

¹Yozgat Bozok University, Sefaatli Vocational School, Türkiye

Keywords

Inventory
Digital Preservation
Digital Archiving
Cultural Heritage
Digital Cultural Heritage

Research Article

DOI:10.53093/mephoj.1200146

Received: 06.11.2022

Revised: 27.11.2022

Accepted: 28.11.2022

Published:22.12.2022

Abstract

Since mankind began to adapt to settled life, it has established various settlements. In these areas, they have built many structures for accommodation and social activities. Some of these structures are still in use today, but most of them are waiting to be underground for various natural or unnatural reasons or have been destroyed due to indifference. Survey studies play an important role in documenting, protecting and transferring cultural heritages that have survived for centuries or that were found during archaeological excavations. The cultural heritage handed down to us from past societies must be preserved for the benefit of all. In the era of globalization, cultural heritage helps us remember our cultural diversity and its understanding fosters mutual respect and renewed dialogue between different cultures. Transferring the cultural heritage that has survived from the past to the present to the societies that will live after us, without any change in its essence, contributes both to the development of a country and to new works to be done. A country's economic growth and social progress present both challenges and opportunities for the preservation of cultural heritage. In this study, the documentation and survey sample study of Seyfeddin Karasungur tomb in Konya province was carried out. For the documentation work, a 3D model of the building was obtained in terrestrial photogrammetry software with pictures taken from various angles.

1. Introduction

Cultural Heritage is an expression of lifestyles developed by a community, including its traditions, and transmitted from generation to generation, including practices, places, objects, artistic expressions and values. Cultural Heritage is generally expressed as tangible or intangible cultural heritage [1-2]. The most important examples of tangible cultural heritage are architectural works that reflect the life style of a society [3-4].

Documentation is the process of collecting and recording all information, in both written and visual form, obtained during the inspection and repair of a historical building, when necessary, especially for the purpose of documenting cultural artifacts. Documentation allows us to physically preserve a cultural object and, more importantly, it allows us to understand and infer about the past [5-6]. Documentation studies are very important in order to transfer the physical effects of the period and the cultural

environment on the structure to the next generations. In addition, it helps to reflect the cultural understanding of the period to which the work belongs to today's people by documenting the cultural heritages in question [7-9]. Cultural heritage provides a great perspective on how people look at who they are in the fascinating world. In this sense, the importance of documenting cultural heritage is increasing day by day [10-12].

Documentation and survey studies are the first and most important steps in order to preserve the cultural heritage and transfer it to future generations in accordance with its originality [13-15]. A survey is the expression of the current state of the building's interior and exterior architecture, original decoration, carrier system and building materials with scaled drawings in order to closely examine and document the urban texture or archaeological remains of a building, to evaluate it in terms of architectural history, and to prepare restoration projects [16-18].

* Corresponding Author

(adem.kabadayi@bozok.edu.tr) ORCID ID 0000-0002-4891-8131
(alperen.erdogan@bozok.edu.tr) ORCID ID 0000-0003-1240-833X

Cite this article

Kabadayı, A., & Erdoğan, A. (2022). Application of terrestrial photogrammetry method in cultural heritage studies: A case study of Seyfeddin Karasungur. *Mersin Photogrammetry Journal*, 4(2), 62-67

Today, documentation of cultural assets is done quickly and reliably with the photogrammetry technique [19-21]. With the digital photogrammetric method, the documentation, presentation, protection of historical buildings, and the detection of deteriorations that may occur in the works during and after the restoration works can be determined by the conservation experts [22-24]. Another important advantage of photogrammetry is that it allows 3D representation of objects by modeling them in accordance with their originals [25-26].

With this study, the use of Photogrammetry in Engineering and Architectural studies will increase its effectiveness in current application areas in parallel with the developments in science and technology, as well as provide application opportunities in many other areas. In addition, a survey and 3D modeling of the Historic Dome was carried out with millimeter-precision measurements and terrestrial photogrammetry technique, which can serve as a basis for architecture, restoration, restitution, documentation and registration of historical monuments.

2. Method

2.1. Seyfeddin Karasungur Shrine

Emir Seyfettin Karasungur is the contemporary of Hz. Mevlana. His exact date of birth and death is unknown. He is the brother of Celaledin Karatay, who lived in the 1200s during the Seljuk period and gave his name to the Karatay District.

Seyfeddin Karasungur established a madrasah on the site of his tomb in the current Çiftemerdiven District and was its patron for years. After the madrasa was demolished, it was built on the site of the current Karasungur Tomb. The date of his death, the architect of the tomb and the date of its construction are not known exactly.

The tomb is located in the center of Konya, at 37.874937° North latitude, 32.495539° East longitude, in Çifte Merdiven neighborhood. It is on an octagonal base, has an octagonal body and two floors, and is covered with a dome from the inside and a pyramidal cone from the outside. The main entrance door of the tomb is located on the east side, but this door has been canceled today and a new door and a window on the door has been opened on the west side. The main door, placed in a deep niche with a pointed arch, is limited by a high rectangular frame. The upper floor, which has an octagonal plan, is covered with a dome crossed with squinches. On the upper part of each façade, there is a thin and long rectangular window. There is a coffin inside. Today, it is not possible to enter the lower floor, which is completely underground. Stone, brick and marble were used as building materials in the tomb. The original door of the tomb is covered with marble. The dome, the cone, the skirt of the cone and the corners of the octagon are made of bricks. The rectangular panels on each exterior façade are covered with cut stone, arches on the windows and geometric decorations on the other surfaces are carved on the stone surfaces with the scraping technique. In the interior, the lower parts of the walls are rubble and the upper parts are brick.



Figure 1. Location map of the study area

2.2. Field study

Topcon GPT 7003i total station (Figure 2) measuring devices were used for field measurement and Nikon D5100 camera was used for photographing.



Figure 2. Topcon-gpt-7003i (url-4)

Before the field measurements in the field, the locations of the polygon points to be established around it were determined and their installation was made on the ground in order to measure the cultural heritage to be documented. The coordinates of the polygon points established in such a way that they can see each other are taken in the national coordinate system with the GNSS receiver with CORS-TR connection. By making polygon balancing with the total station on these polygon points, the measurement was continued by providing an accuracy of less than 0.5 cm. In addition, the picture of the building was taken and the reference points made on the building with the total station device were marked on the picture.

The measurement process of the study was completed in about an hour. Photographs were taken to see all sides of the building. At least 3 photographs have been taken from one side, the photographs taken are overlapped and have different shooting points. Photo shoot was completed in such a way that the focal length of the camera was fixed without zooming in.

2.3. Office Work

The values of the reference points made on the building in the project area were transferred in ncn format from the total station device, shown in Figure 2 and the properties of which are specified in Table 1. The camera used in photographing is shown in Figure 3, and the characteristics of the camera are given in Table 2. The polygon mesh is given in Figure 4. The data transferred from Totalstation was converted into txt format by Netcad 5.2 software, and the file was transferred to Photomodeler (PM) software and used to balance the

pictures in a coordinated manner. The parameters of the camera were introduced to the PM software and the calibration process was carried out. For the calibration process, sample template papers were printed in A4 size in PM software. 10 photographs of the calibration paper were taken. After the calibration process, the balancing process was carried out successfully and the drawing process was started.

Table 1. Topcon-gpt-7003i features

Field of view	1° 30 ×
min. Focal Distance	1,3 m (4,29 ft.)
Measuring range	1,5 - 250m (5 - 820 ft.)
Measurement Display	11 steps
Laser Class	Class1 (disntaj measurement) Class 2 (Lazer Sign On)
Battery	4400 mAH Including distance measurement: Approx. 5 hours
Maximum uptime	Angle measurement only: Approx. 10 hours
Charging Time	4 hours



Figure 3. Digital Handheld Camera

Table 2. Properties of the camera

Weight	226 g
Turkish Language/ Digital Display	Yes/Yes
Video Record/ Wifi	Yes/Yes
Megapixel	14.2
Image resolution	4320 x 3240
Optical/Digital zoom	18x / Yes
Sensor width	6.16 mm
Sensor resolution width	4346 piksel
Pixel pitch	1.42 µm
Pixel density	49.78 MP / cm ²
Storage type	SD/SDHC/ SDXC

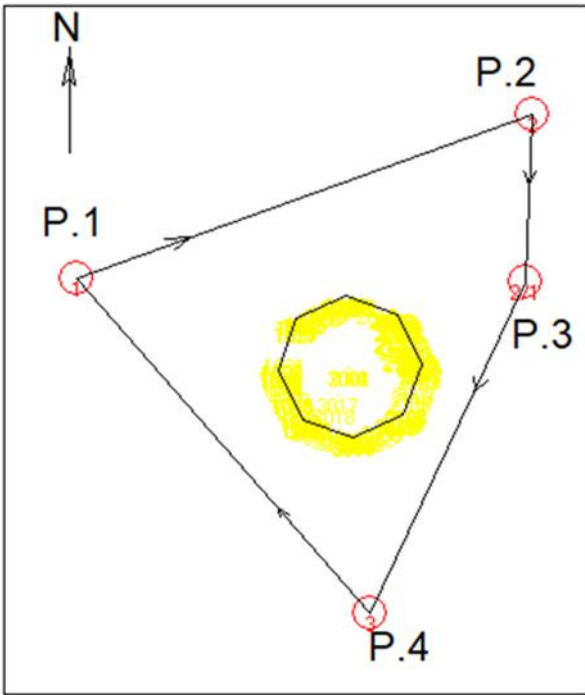


Figure 4. Polygon mesh

The top view of the drawing made from the stabilized photographs made in PM software is given in [Figure 4](#), the front view is given in [Figure 5](#), and the side view is given in [Figure 6](#). After the drawing was made, the surface coating was made, given in [Figure 8](#). In [Figure 7](#), there is a height analysis of the building whose 3D model is made. The drawing of the main lines of the building in PM software has been completed with high precision.

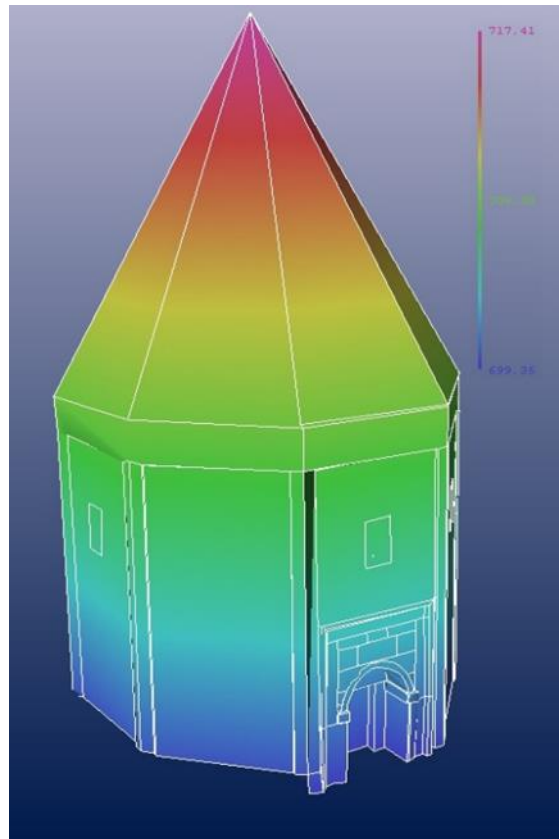


Figure 8. The height analysis of the tomb, which was drawn in PM software

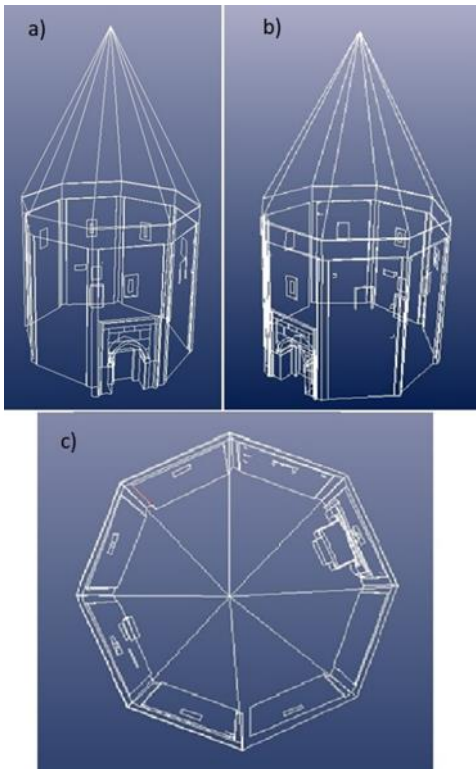


Figure 5. a) Front view of the tomb drawn in PM software, b) Side view of the tomb drawn in PM software c) Top view of the tomb drawn in PM software

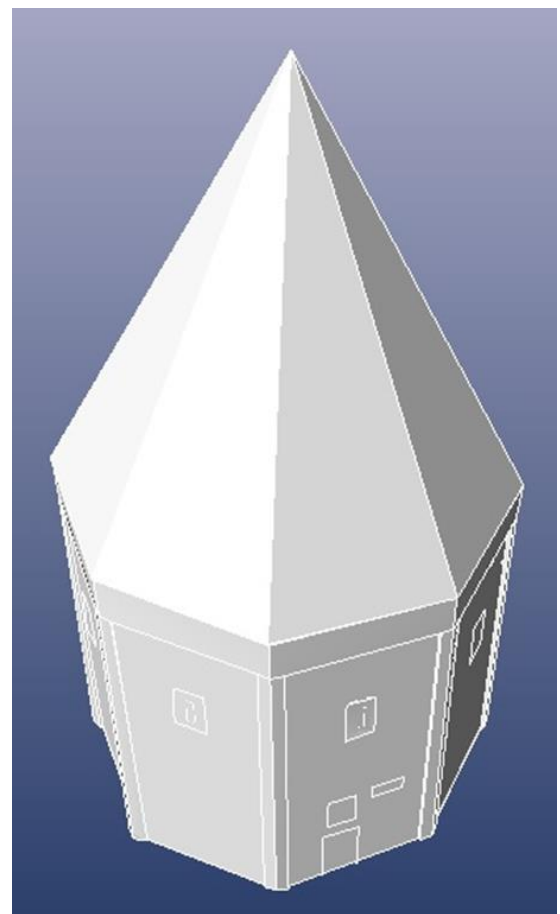


Figure 9. Surface coated view of the tomb drawn in PM software



Figure 10. Surface coated and picture dressed view of the tomb drawn in PM software

3. Conclusion

Terrestrial photogrammetry technique, which is the most effective method in documenting historical artifacts, is superior to classical methods in terms of time, cost and accuracy. The fact that field data can be collected with a simple handheld camera and that classical surveying techniques are supportive play a major role in the preference of this method. With the 3D model we created from the data obtained by this method used in the documentation of Seyfeddin Karasungur Cupola, every detail of the structure was drawn in its real size. Then, these drawings were covered with the help of photographs taken in the field, and the real image of the surface was obtained as a 3D model. Extremely sensitive measurements can be made on the model of the work and it can be easily used in restoration projects.

Author contributions

Adem Kabadayı: Literature review, Field study, Modelling, Writing; **Alperen Erdoğan:** Editing

Conflicts of interest

The authors declare no conflicts of interest.

References

1. ICOMOS (2002). International Cultural Tourism Charter. Principles And Guidelines for Managing Tourism at Places of Cultural And Heritage Significance. ICOMOS International Cultural Tourism Committee.
2. Uysal, M., Polat, N., Toprak, A. S., & Yakar, M. (2013). 3D Modeling of Historical Doger Caravansaries by Digital Photogrammetry. *Remote Sensing and Spatial Information Sciences Volume XL-5/W2*.
3. Kaya, Y., Yiğit, A. Y., Ulvi, A., & Yakar, M. (2021). Arkeolojik Alanların Dokümantasyonunda Fotogrametrik Tekniklerinin Doğruluklarının Karşılaştırmalı Analizi: Konya Yunuslar Örneği. *Harita Dergisi* 87 (165), 57-72.
4. Yakar, M., & Yılmaz, H. M. (2008). Kültürel miraslardan tarihi Horozluhan'ın fotogrametrik rölöve çalışması ve 3 boyutlu modellenmesi. *Selçuk Üniversitesi Mühendislik, Bilim ve Teknoloji Dergisi*, 23(2), 25-33
5. Ulvi, A., Yiğit, A. Y., & Yakar, M. (2019). Modeling of Historical Fountains by Using Close-Range Photogrammetric Techniques. *Mersin Photogrammetry Journal*, 1(1), 1-6.
6. Yakar, M., Kabadayı, A., Yiğit, A. Y., Çıkıkcı, K., Kaya, Y. & Catin, S. S. (2016). Emir Saltuk Kümbeti Fotogrametrik Rölöve Çalışması Ve 3Boyutlu Modellenmesi. *Geomatik*, 1 (1), 14-18.
7. Asri, İ., & Çorumluoğlu, Ö. (2007). Büyük Objelerde Tarihi Dokümantasyon ve Tanıtım Amaçlı Gpsit Destekli Digital Fotogrametrik 3b Modelleme.
8. Kabadayı, A., Yunus, K. & Yiğit, A. Y. (2020). Comparison of documentation cultural artifacts using the 3D model in different software. *Mersin Photogrammetry Journal*, 2(2), 51-58.
9. Ulvi, A., Yakar, M., Yiğit, A. Y. & Kaya, Y. (2020). İHA ve yersel fotogrametrik teknikler kullanarak Aksaray Kızıl Kilise'nin 3 boyutlu nokta bulutu ve modelinin üretilmesi, *Geomatik*, 5, 1, 22-30.
10. Şasi, A. & Yakar, M. (2018). Photogrammetric modelling of Hasbey Dar'ülhuffaz (Masjid) using an unmanned aerial vehicle. *International Journal of Engineering and Geosciences*, 3 (1), 6-11.
11. Yılmaz, H. M., Yakar, M., Gulec, S. A., & Dulgerler, O. N. (2007). Importance of digital close-range photogrammetry in documentation of cultural heritage. *Journal of Cultural Heritage*, 8(4), 428-433.
12. Yakar, M. (2011). Using close range photogrammetry to measure the position of inaccessible geological features. *Experimental Techniques*, 35(1), 54-59.
13. Mırdan, O. & Yakar, M. (2017). Tarihi Eserlerin İnsansız Hava Aracı ile Modellenmesinde Karşılaşılan Sorunlar. *Geomatik*, 2 (3), 118-125.
14. Kanun, E., Alptekin, A., & Yakar, M. (2022). Cultural heritage modelling using UAV photogrammetric methods: a case study of Kanlıdivane archeological site. *Advanced UAV*, 1(1), 24-33

15. Yakar, M., Yılmaz, H., Yıldız, F., Zeybek, M., Şentürk, H. & Çelik, H. (2010). Silifke-Mersin Bölgesinde Roma Dönemi Eserlerinin 3 Boyutlu Modelleme Çalışması ve Animasyonu. Jeodezi ve Jeoinformasyon Dergisi, (101).
16. Doğan, Y. & Yakar, M. (2018). GIS and three-dimensional modeling for cultural heritages. International Journal of Engineering and Geosciences, 3 (2), 50-55.
17. Şahin, İ., & Yakar, M. (2008). Farklı kaynaklardan elde edilen sayısal yükseklik modellerinin ortofoto doğruluğuna etkilerinin araştırılması. Harita Dergisi, 74(140), 45-59.
18. Alptekin, A. & Yakar, M. (2020). Heyelan bölgesinin İHA kullanarak modellenmesi. Türkiye İnsansız Hava Araçları Dergisi, 2 (1), 17-21
19. Yakar, M., & Yılmaz, H. M. (2011). Determination of erosion on a small fairy chimney. Experimental Techniques, 35(5), 76-81.
20. Yakar, M. & Doğan, Y. (2017). Mersin Silifke Mezgit Kale Anıt Mezarı Fotogrametrik Rölöve Alımı Ve Üç Boyutlu Modelleme Çalışması. Geomatik, 2 (1), 11-17.
21. Yakar, M., Yılmaz, H. M., Güleç, S. A., & Korumaz, M. (2009). Advantage Of Digital Close-Range Photogrammetry İn Drawing of Muqarnas İn Architecture'. Information Technology Journal, 8 (2), 202-207.
22. Yakar, M., & Mohammed, O. (2016). Yersel Fotogrametrik Yöntem ile İbadethanelerin Modellenmesi. Journal of Technical-Online, 15(2).
23. Kanun, E., & Yakar, M. (2021). Mobile phone-based photogrammetry for 3D modeling of ship hulls. Mersin University Journal of Maritime Faculty, 3(1), 9-16.
24. Alptekin, A., Çelik, M. Ö., & Yakar, M. (2019). Anıtmezarın yersel lazer tarayıcı kullanarak 3B modellenmesi. Türkiye Lidar Dergisi, 1(1), 1-4.
25. Yılmaz, H. M., Aktan, N., Çolak, A. & Alptekin, A. (2022). Modelling Ozancık village (Aksaray) in computer environment using UAV photogrammetry. Mersin Photogrammetry Journal, 4 (1), 32-36. DOI: 10.53093/mephoj.1132303
26. Kaya, Y., Şenol, H. İ. & Polat, N. (2021). Three-dimensional modeling and drawings of stone column motifs in Harran Ruins. Mersin Photogrammetry Journal, 3 (2), 48-52.



© Author(s) 2022. This work is distributed under <https://creativecommons.org/licenses/by-sa/4.0/>



Mersin Photogrammetry Journal

<https://dergipark.org.tr/en/pub/mephoj>

e-ISSN 2687-654X



The use of unmanned aerial vehicle (UAV) data in village development plans: A case study of Aksaray Yaylak Village

Hacı Murat Yılmaz^{*1}, Nusret Aktan², Adem Çolak², Aydın Alptekin³

¹Aksaray University, Geomatics Engineering Department, Türkiye

²Aksaray Special Provincial Administration, Aksaray, Türkiye

³Mersin University, Geological Engineering Department, Türkiye

Keywords

UAV
Terrain modelling
DSM
Orthophoto

Research Article

DOI:10.53093/mephoj.1202261

Received: 10.11.2022

Revised: 28.11.2022

Accepted: 19.12.2022

Published: 22.12.2022

Abstract

With the increasing population, the problem of people's need for shelter has also emerged. In many settlements, structures were built without the necessary planning. Three-dimensional (3D) models of these lands should be created in order to make land management plans. Technological improvements in remote sensing have made easier the terrain modelling. To make a better land management plan of rural areas, we need high resolution maps. Unmanned aerial vehicle (UAV) is one of the methods in map production, which can obtain spatial data with high accuracy. In this study, we created 3D model of Yaylak village located in Aksaray District using UAV Photogrammetry. We created high resolution Digital Surface Map and orthophoto map of the village using the pictures obtained from e-Bee. Using these maps, the administrator of the region will decide healthy decision. This study shows us UAV can be used in preparing the necessary maps for designing the settlement area.

1. Introduction

Turkey is a country whose population is increasing every year. The needs of this growing population are also increasing. The need for shelter is one of them. In many regions, rapid construction was carried out in order to provide housing to the rapidly increasing population as soon as possible. This situation has led to the construction of buildings without making the necessary plans in a healthy way. Today, we see the consequences of not making a healthy plan in the past. Disruptions in infrastructure services, narrow roads in transportation and various problems in land use draw attention.

The development of technology has caused the peaceful life in countries with high civilization level to be known by the people in the village. This situation has led to an increase in the demands and studies have started to bring the village life to a better quality. In order to carry out these studies, the three-dimensional (3D) model of the land must be seen in the computer environment. It is not an easy task to prepare map of the wide terrain as it requires long field survey. UAV has made survey engineers life easier [1]. Using a UAV has many

advantages as it is time-consuming and allows high accuracy in modelling the terrain [2]. The camera mounted on the UAV provides high resolution pictures [3]. Spatial data can be obtained using UAV with high precision and accuracy.

Classical photogrammetry techniques have some accuracy problems in large areas. Advances in remote sensing technology overcomes this problem. UAVs are economical, easy to use and practical in steep terrain [4]. Therefore, in the last two decades, UAV has been used in engineering projects frequently. Rockfall [5], landslide [6], cultural heritage [7], material deterioration [8] and terrain modelling [9-10] are the main topics which used UAV photogrammetry.

In Turkey, most village sites are poorly organized. When people found a place to construct a one-story house, they build the house without any management plan. Randomly designed buildings cause too many problems. In this study, we tried to create the actual orthophoto and DSM of a village site located in Aksaray district, Turkey (Figure 1). To generate modern settlement areas, mapping the terrain is a very important task.

* Corresponding Author

(hmuraty@gmail.com) ORCID ID 0000-0002-9725-5792
(nusretaktan@hotmail.com) ORCID ID 0000-0003-2582-9395
(acolak68@hotmail.com) ORCID ID 0000-0003-2582-9395
(aydinalptekin@mersin.edu.tr) ORCID ID 0000-0002-5605-0758

Cite this article

Yılmaz, H. M., Aktan, N., Çolak, A., & Alptekin, A. (2022). The use of unmanned aerial vehicle (UAV) data in village development plans: A case study of Aksaray Yaylak Village. *Mersin Photogrammetry Journal*, 4(2), 68-72

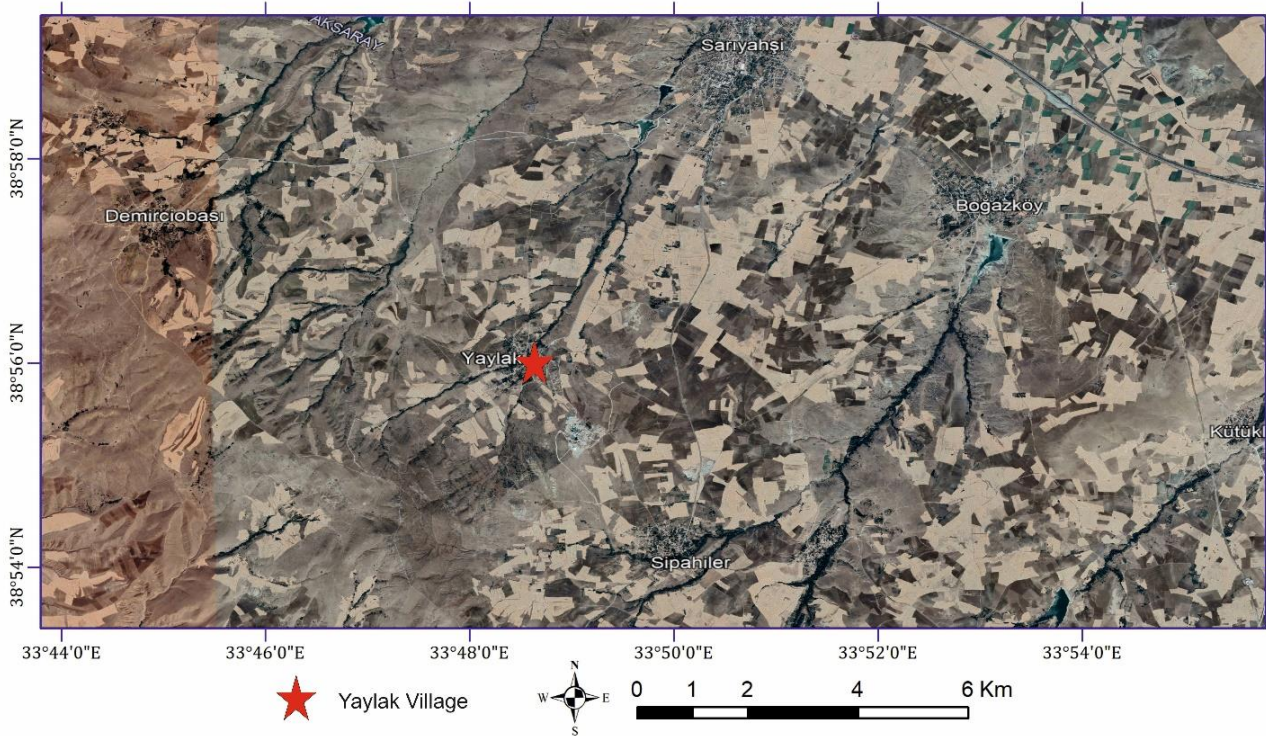


Figure 1. Location map of study map

2. Method

In order to create the risk management plan of the village site, high resolution maps are needed. One of the methods adopted in order to obtain the spatial data needed in recent years is the use of UAVs. UAV photogrammetry enables us to create the necessary maps in a short time. The software used in processing the pictures is improving.

With the photogrammetry technique, we can create 3D models of objects without touching them and without causing any damage to them. Terrestrial photogrammetry is a time-consuming method. Airborne photogrammetry is very useful when compared to terrestrial photogrammetry.

Turkey has very rough terrains due to its geographical location and geomorphological features. This situation both causes many natural disasters and prevents the settlement plans to be made in a healthy way.

In this study, we used eBee SenseFly with real-time kinematic positioning feature (Figure 2) to model the terrain. We prepared the flight mission and get the pictures. A wide area covering 2.7824 km² has been modelled using 814 pictures. Average ground sampling distance was 2.88 cm. We used Pix4D Mapper to produce models in a short time.

UAV photogrammetry enables the engineer's duty as it can gather data from terrain in a short time.

The lower the flight is made in UAV photogrammetry, the clearer the model will be. Since the e-bee has a high camera resolution, this problem has disappeared. The lower the flight height, the higher the number of images.

Structure from motion (SfM) algorithm creates 3D modelling of the terrain from 2D pictures. This algorithm creates a model of the terrain by finding common points on consecutive pictures. The results of processing options are given in Table 1.

The results of DSM, orthomosaic and index details are given in Table 2.

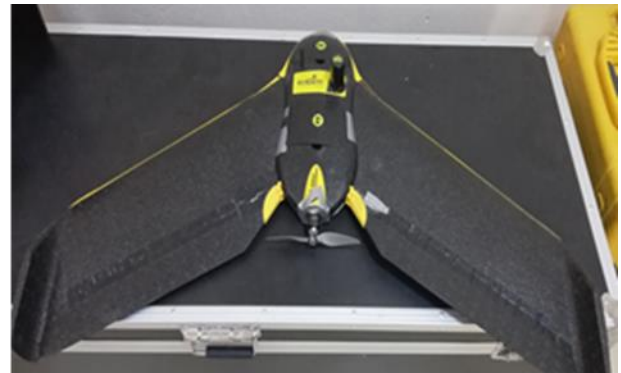


Figure 2. eBee SenseFly

Table 1. Processing options

Property	Value
Image Scale	multiscale, 1/2 (Half image size, Default)
Point Density	Optimal
Minimum Number of Matches	3
3D Textured Mesh Generation	yes
3D Textured Mesh Settings	Resolution: Medium Resolution (default)
	Color Balancing: no
	LOD Generated: no
LOD	
Advanced: 3D Textured Mesh Settings	Advanced: 3D Textured Mesh Settings Sample Density
	Divider: 1
	group1
Advanced: Image Groups	yes
Advanced: Use Processing Area	yes
Advanced: Use Annotations	yes
Time for Point Cloud Densification	04h:35m:46s
Time for 3D Textured Mesh Generation	01h:04m:31s

Table 2. Index details

Property	Value
DSM and Orthomosaic Resolution	1 x GSD (2.88 [cm/pixel])
DSM Filters	Noise Filtering: yes
	Surface Smoothing: yes, Type: Sharp
Raster DSM	Generated: yes
	Method: Inverse Distance Weighting
	Merge Tiles: yes
Orthomosaic	Generated: yes
	Merge Tiles: yes
	GeoTIFF Without Transparency: no
	Google Maps Tiles and KML: no
Grid DSM	Generated: yes, Spacing [cm]: 100
Time for DSM Generation	02h:12m:37s
Time for Orthomosaic Generation	05h:19m:50s

3. Results and Discussion

UAV technology and applications are increasingly used by organizations and academic society in the last decade.

Rural areas are surrounded by high mountains. This causes too many problems. UAV photogrammetry makes people's lives easier. 3D modeling of the land in high resolution provides great convenience to decision makers. The more detailed data we can see comfortably in the computer environment, the healthier we can make decisions. UAV technology allows us to prepare a 3D model of the terrain in high resolution. Completing both the field work and the modeling process in a short time

is the most important reason for us to use UAV technology.

As a result of this study, Digital Surface Map (DSM) (Figure 3) and orthophoto (Figure 4) were produced in high resolution. DSM will show us the slope structure of the land and the water flow network.

Laser scanning method is also used in terrain modeling. Terrain models using airborne lidar have emerged in recent years. The fact that this method is expensive and the fieldwork and modeling processes are difficult and long makes it not preferred. Satellite image modelling is also an important element in terrain modelling. However, it is very expensive when compared to UAV technology.

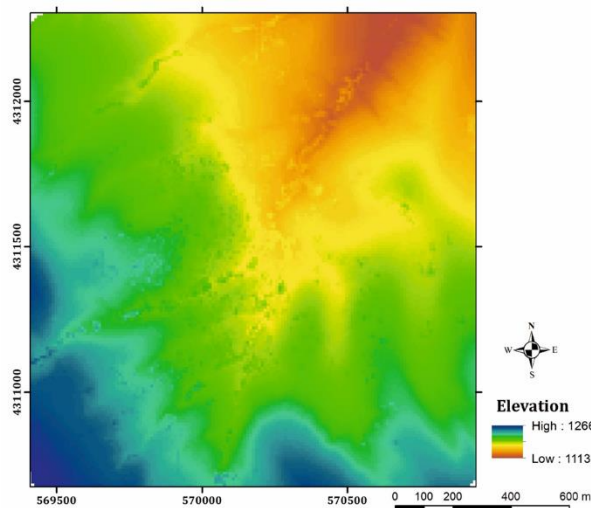


Figure 3. DSM

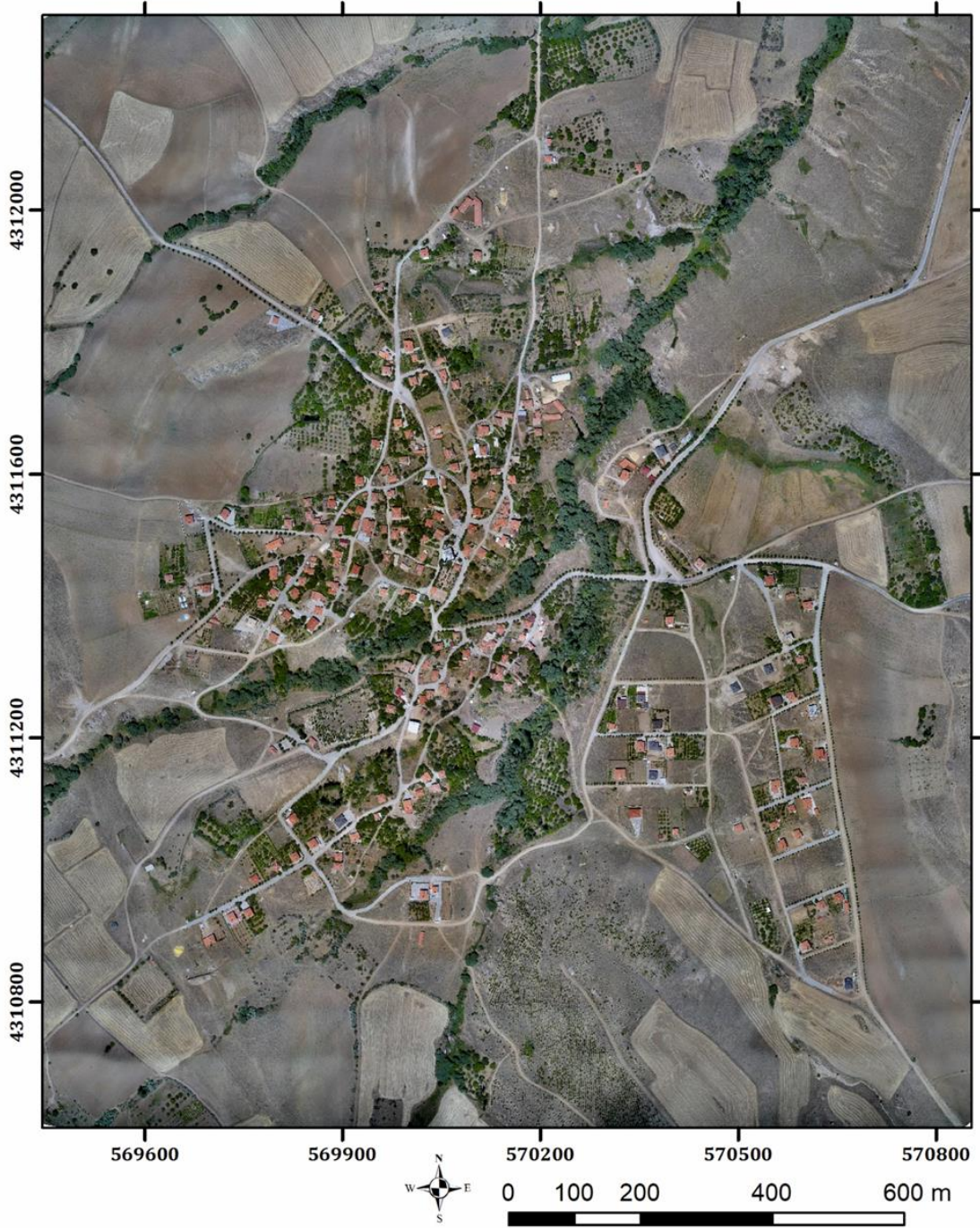


Figure 4. Orthophoto

4. Conclusion

In this study, we modelled a village using UAV technology with high resolution. We have quickly modeled a large terrain using 814 pictures. The development of technology has made our lives easier. A large database has been created for managers. A very high-quality data set has been created that can be used in making decisions that will increase people's quality of life. It will be possible to find solutions to the problems by using scientific methods in the village settlement. A high-quality land management plan can be prepared.

Acknowledgement

We thank Aksaray Special Provincial Administration for enabling us to provide the data.

Author contributions

Hacı Murat Yılmaz: Conceptualization, Methodology, Software
Nusret Aktan: Data curation, Writing-Original draft preparation, Software, Validation.
Adem Çolak: Visualization, Investigation, Writing-Reviewing and Editing.
Aydın Alptekin: Reviewing, Editing

Conflicts of interest

The authors declare no conflicts of interest.

References

1. Alyılmaz, C., Yakar, M., & Yılmaz, H. M. (2010). Drawing of petroglyphs in Mongolia by close range photogrammetry. *Scientific Research and Essays*, 5(11), 1216-1222.
2. Yılmaz, H. M., Mutluoğlu, Ö., Ulvi, A., Yaman, A. & Bilgilioğlu, S. S., (2018). İnsansız Hava Aracı ile Ortofoto Üretimi ve Aksaray Üniversitesi Kampüsü Örneği. *Geomatik Dergisi*, 3(2), 129-136
3. Alptekin, A., ÇELİK, M. Ö., KUŞAK, L., Ünel, F. B., & Yakar, M. (2019). Anafi Parrot'un heyelan bölgesi haritalandırılmasında kullanımı. *Türkiye İnsansız Hava Araçları Dergisi*, 1(1), 33-37.
4. Yakar, M., & Doğan, Y. (2017). Silifke Aşağı Dünya Obruğunun İHA Kullanılarak Üç Boyutlu Modellenmesi. *Afyon Kocatepe Üniversitesi Fen ve Mühendislik Bilimleri Dergisi*, 17(4), 94-101.
5. Alptekin, A., Çelik, M. Ö., Doğan, Y., & Yakar, M. (2019). Mapping of a rockfall site with an unmanned aerial vehicle. *Mersin Photogrammetry Journal*, 1(1), 12-16.
6. Alptekin, A., & Yakar, M. (2020). Heyelan bölgesinin İHA kullanarak modellenmesi. *Türkiye İnsansız Hava Araçları Dergisi*, 2(1), 17-21.
7. Alptekin, A., & Yakar, M. (2021). 3D model of Üçayak Ruins obtained from point clouds. *Mersin Photogrammetry Journal*, 3(2), 37-40.
8. Karataş, L., Alptekin, A., Kanun, E., & Yakar, M. (2022). Tarihi kârgir yapılarda taş malzeme bozulmalarının İHA fotogrametrisi kullanarak tespiti ve belgelenmesi: Mersin Kanlıdivane ören yeri vaka çalışması. *İçel Dergisi*, 2(2), 41-49.
9. Alptekin, A., & Yakar, M. (2020). Determination of pond volume with using an unmanned aerial vehicle. *Mersin Photogrammetry Journal*, 2(2), 59-63.
10. Ünel, F. B., Kuşak, L., Çelik, M., Alptekin, A., & Yakar, M. (2020). Kıyı çizgisinin belirlenerek mülkiyet durumunun incelenmesi. *Türkiye Arazi Yönetimi Dergisi*, 2(1), 33-40.



© Author(s) 2022. This work is distributed under <https://creativecommons.org/licenses/by-sa/4.0/>